serum were purchased from Invitrogen (Carlsbad, CA). 3FLAG-4F2hc cDNA was provided by Yoshikatsu Kanai. All other reagents were of analytical grade.

Split-ubiquitin membrane yeast two-hybrid screening system. DUALmembrane kit 3 (Dualsystems Biotech), the split-ubiquitin membrane yeast two-hybrid system, was used to identify the protein associating with GLUT1. Briefly, in this system, the bait is fused to the COOH-terminal half of ubiquitin (Cub) and the artificial transcription factor LexA-VP16. The prey is fused to the mutated NH_2-terminal half of ubiquitin (NubG). If the bait and prey interact, split ubiquitins are reconstituted and recognized by ubiquitin-specific proteases. Then, the artificial transcription factor consisting of Cub and LexA-VP16 is released and moves to the nucleus, leading to reporter gene activation (Fig. 1*A*).

Rabbit GLUT1 cDNA was inserted into the expression vector pBT3-STE to generate the fusion bait with the split ubiquitin and an artificial transcriptional factor (Cub-LexA-VP16) to the COOH terminus of GLUT1. Mouse heart cDNA library, inserted into a pDL2xN-SUC/pDL2xN-STE vector, was purchased from Dualsystems Biotech, and then screened. Bait and the mouse heart cDNA library were transformed into yeast strain NMY51. The HIS3 reporter construct was assayed by growth on SD-Trp-Leu-His-Ade drop-out plates supplemented with 2.5 mM 3-amino-1,2,4-triazole (Wako). Qualitative assessment of the lacZ reporter was conducted using filter lift galactosidase assays (8).

Cell culture, expression vectors, adenovirus generation, and small interfering RNA transfections. HepG2 hepatoma cells, HeLa cells, and human embryonic kidney (HEK293) cells were grown in DMEM containing 10% fetal calf serum at 37°C in 5% (vol/vol) CO_2 in air. Rabbit GLUT1-HA, rat GLUT4-HA, rabbit GLUT1-DsRed, human LAT1-DsRed, green fluorescent protein (GFP)-human 4F2hc, and human 4F2hc were inserted into cloning sites in the mammalian expression vector pcDNA3 (Invitrogen), as reported previously (34). Transfection of these expression vectors was performed by the lipofection method using FuGENE 6 (Roche Applied Science, Indianapolis, IN). Recombinant adenovirus, encoding mouse 4F2hc, was generated according to the instruction manual of the Adenovirus Dual Expression Kit (TaKaRa Bio). Adenovirus encoding LacZ served as a control.

The small interfering RNA (siRNA) against 4F2hc was purchased from Invitrogen (Stealth/siRNA duplex oligoribonucleotides), and the transfection of this siRNA was performed using Lipofectamine RNAiMAX (Invitrogen).

Immunoprecipitation and immunoblotting. Whole cell extracts were prepared from HEK293 cells overexpressing 3FLAG-4F2hc, GLUT1-HA, or GLUT4-HA in lysis buffer [50 mM Tris·HCl, pH 7.5, 150 mM NaCl, 10% (wt/vol) glycerol, 100 mM NaF, 10 mM EGTA, 1 mM Na_3VO_4, 1% (wt/vol) Triton X-100, 5 μM $ZnCl_2$, 2 mM phenylmethylsulfonyl fluoride (PMSF), 10 μg/ml aprotinin, and 1 μg/ml leupeptin]. Cell extracts were incubated for 4 h at 4°C with the HA antibody and then for 1 h with 30 μl of protein G-Sepharose beads. The pellets were washed five times with 1 ml of lysis buffer, resuspended in Laemmli sample buffer, and subjected to SDS-polyacrylamide gel electrophoresis (SDS-PAGE).

HeLa cells were preincubated with 2.5 mM DSP (Thermo Scientific) for 30 min. Male mice, 9 wk of age, were obtained from the Nippon Bio-Supply Center (Tokyo, Japan). All animal studies were conducted according to the Japanese guidelines for the care and use of experimental animals, and the experimental protocols were approved by the Committee of Research Facilities for Laboratory Animal Science, Natural Science Center for Basic Research and Development (N-BARD), University of Hiroshima. For preparation of the membrane fraction, HeLa cells and mouse whole brains were homogenized with homogenizing buffer (0.25 M sucrose, 10 mM Tris, 1 mM EDTA). After filtration through a nylon membrane, the lysates were centrifuged at 600 *g* for 10 min, and the supernatant was centrifuged at 3,000 *g* for 10 min. Then, the supernatant was centrifuged at 30,000 *g* for 30 min, and the pellet was resuspended in 10 mM Tris, 1 mM EDTA, at pH 7.4.

The 4F2hc antibody (90 μg) or control IgG (90 μg) was covalently coupled to 20 μl of IPeX beads (Gene Bio-Application) and stabilized for 30 min at room temperature. Then, the solubilized membrane fraction (200 μg in 200 μl) was incubated with 5 μl of anti-4F2hc-coupled or anti-IgG-coupled beads for 4 h at 4°C. The beads were extensively washed, and the immunoprecipitated proteins were eluted in Laemmli buffer and resolved by SDS-PAGE.

Western blot analysis was carried out as described previously (34). In brief, equal amounts of protein lysates were separated by SDS-PAGE and electrophoretically transferred to polyvinylidene difluoride membranes in a transfer buffer consisting of 20 mM Tris·HCl, 150 mM glycine, and 20% methanol. The membranes were blocked with 3% nonfat dry milk in Tris-buffered saline with 0.1% Tween 20 and incubated with specific antibodies, followed by incubation with horseradish peroxidase-conjugated secondary antibodies. The antigen-antibody interactions were visualized by incubation with ECL chemiluminescence reagent (GE Healthcare).

Measurement of 2-deoxyglucose and leucine uptakes. The 2-deoxy-D-[^{3}H]glucose uptake assay was performed as described previously (2). HeLa or HepG2 cells were incubated in serum-free DMEM for 2 h, rapidly washed at 37°C with KRP buffer (in mM: 128 NaCl, 4.7 KCl, 1.25 $CaCl_2$, 1.25 $MgSO_4$, 10 $NaHPO_4$, pH 7.4), and 450 μl of KRP buffer were then added to each well. The measurements of 2-deoxyglucose uptake were initiated by addition of 50 μl of 2-deoxy-D-[1, 2-^{3}H]glucose, so that each well contained 0.4 μCi and 0.1 mM 2-deoxyglucose. After a 5-min incubation at 37°C, 1 ml of ice-cold phosphate-buffered saline (PBS) containing 10 mM glucose and 0.3 mM phloretin was added, and the cells were rapidly washed three times with ice-cold PBS containing 10 mM glucose and subsequently solubilized by adding SDS (final concentration, 0.05%). Aliquots of the solubilized extract were assayed for radioactivity using a liquid scintillation counter.

The [^{14}C]L-leucine uptake experiments were performed by essentially the same method as those of 2-deoxy-D-[^{3}H]glucose uptake, with a few modifications (18). Instead of KRP buffer, Na^+-free uptake solution (in mM: 125 choline Cl, 4.8 KCl, 1.3 $CaCl_2$, 1.2 $MgSO_4$, 25 HEPES-Tris, 1.2 KH_2PO_4, 5.6 glucose, pH 7.4) was used. After a 1-min incubation with 20 μM (final concentration) [^{14}C]L-leucine, the uptake reaction was terminated by removing the uptake solution followed by washing four times with ice-cold uptake solution.

GLUT1 degradation assay. To observe GLUT1 degradation, 10 μg/μl cycloheximide, an inhibitor of protein synthesis, was added as indicated in RESULTS and figure legends. The GLUT1 expression level was measured by immunoblotting at the indicated time after the addition of cycloheximide. A lysosome inhibitor, chloroquine, 20 μM (Wako), and a proteasome inhibitor, MG-132, 10 μM (Sigma Aldrich), were added to HeLa cells, and their effects on GLUT1 degradation were also examined.

Immunostaining. HeLa cells were fixed with 4% paraformaldehyde for 10 min, rinsed with PBS, and then exposed to 0.2% Triton X-100 in PBS for 5 min. The cells were subsequently incubated for 1 h at room temperature with anti-GLUT1 rabbit antibody (1:100) and anti-4F2hc mouse antibody (1:50). After being washed with PBS five times, FITC-labeled anti-rabbit IgG (1:100) and Cy3-labeled anti-mouse IgG (1:100) were added as the secondary antibodies. Immunofluorescence was visualized with a laser-scanning confocal imaging system.

RNA analysis. RNA extractions were carried out using TRIzol followed by purification over a QIAEASY RNA column. Reverse transcription and quantitative PCR were carried out as already described. Amplifications of GLUT1 and GAPDH cDNAs were performed using the Opticon Monitor (version 3; Bio-Rad). Cycling conditions comprised a 3-min denaturation step at 95°C, followed by 40 cycles of denaturation (95°C for 15 s), annealing (60°C for 30 s),

and extension (72°C for 30 s). After amplification, melting curve analysis was performed. Each sample was amplified in triplicate.

The primer sets for human (h)GLUT1 were TCACTGTGCTCCTGGTTCTG and CCTGTGCTCCTGAGAGATCC (233 bp) and for hGAPDH were ACCACAGTCCATGCCATCAC and TCCACCACCCTGTTGCTGTA (451 bp).

Statistical analysis. Results are expressed as means ± SE, and statistical comparisons among groups were carried out using Student's *t*-test, unless otherwise indicated.

RESULTS

Identification of 4F2hc, as a novel membrane protein interacting with GLUT1, by the split-ubiquitin membrane yeast two-hybrid system. As bait, full-length GLUT1 was fused to the COOH-terminal half of ubiquitin (Cub) and artificial transcription factors. Expression of the bait in yeast was confirmed by immunoblotting against LexA (Fig. 1*B*). A mouse heart muscle cDNA library, fused to the mutated NH_2-terminal half of ubiquitin (NubG), was screened with the above-mentioned GLUT1 cDNA construct. After the exclusion of nonspecific positive clones, we newly identified 4F2hc as a membrane protein interacting with GLUT1. 4F2hc and GLUT1 coexpressing yeast proliferated in the selective plate (Fig. 1*C*) and exhibited robust β-galactosidase activity (Fig. 1*D*), indicating an interaction between 4F2hc and GLUT1 in yeast.

4F2hc associates and colocalizes with GLUT1. First, FLAG-tagged 4F2hc and either HA-tagged GLUT1 or HA-tagged GLUT4 were overexpressed in HEK293 cells and their associations were examined by coimmunoprecipitation (Fig. 2*A*).

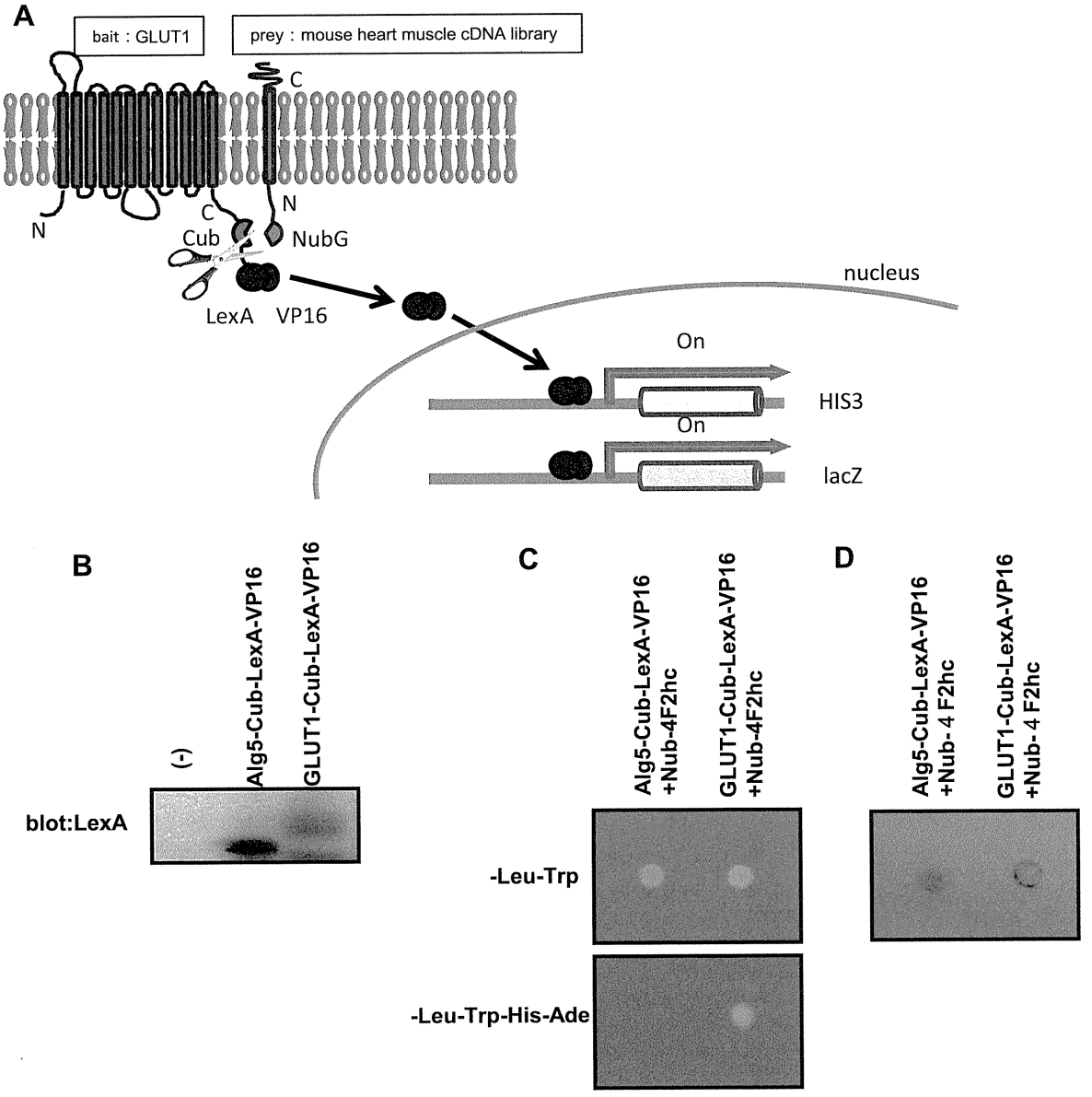

Fig. 1. Using the split-ubiquitin yeast two-hybrid system, 4F2hc was newly identified as a membrane protein interacting with glucose transporter 1 (GLUT1). *A*: split-ubiquitin yeast-two hybrid system. Full-length GLUT1 is fused to the COOH-terminal half of ubiquitin (Cub) and the artificial transcription factor LexA-VP16. Mouse heart muscle cDNA library is fused to the mutated NH_2-terminal half of ubiquitin (NubG). *B*: expression of GLUT1 as bait in yeast. Yeast was subjected to protein extraction before separation of proteins by SDS-PAGE. *C*: yeast coexpressed with Nub-4F2hc and either Alg5-Cub-LexA-VP16 or GLUT1-Cub-LexA-VP16 was incubated on a selective plate for 72 h. *D*: color development in a β-galactosidase assay.

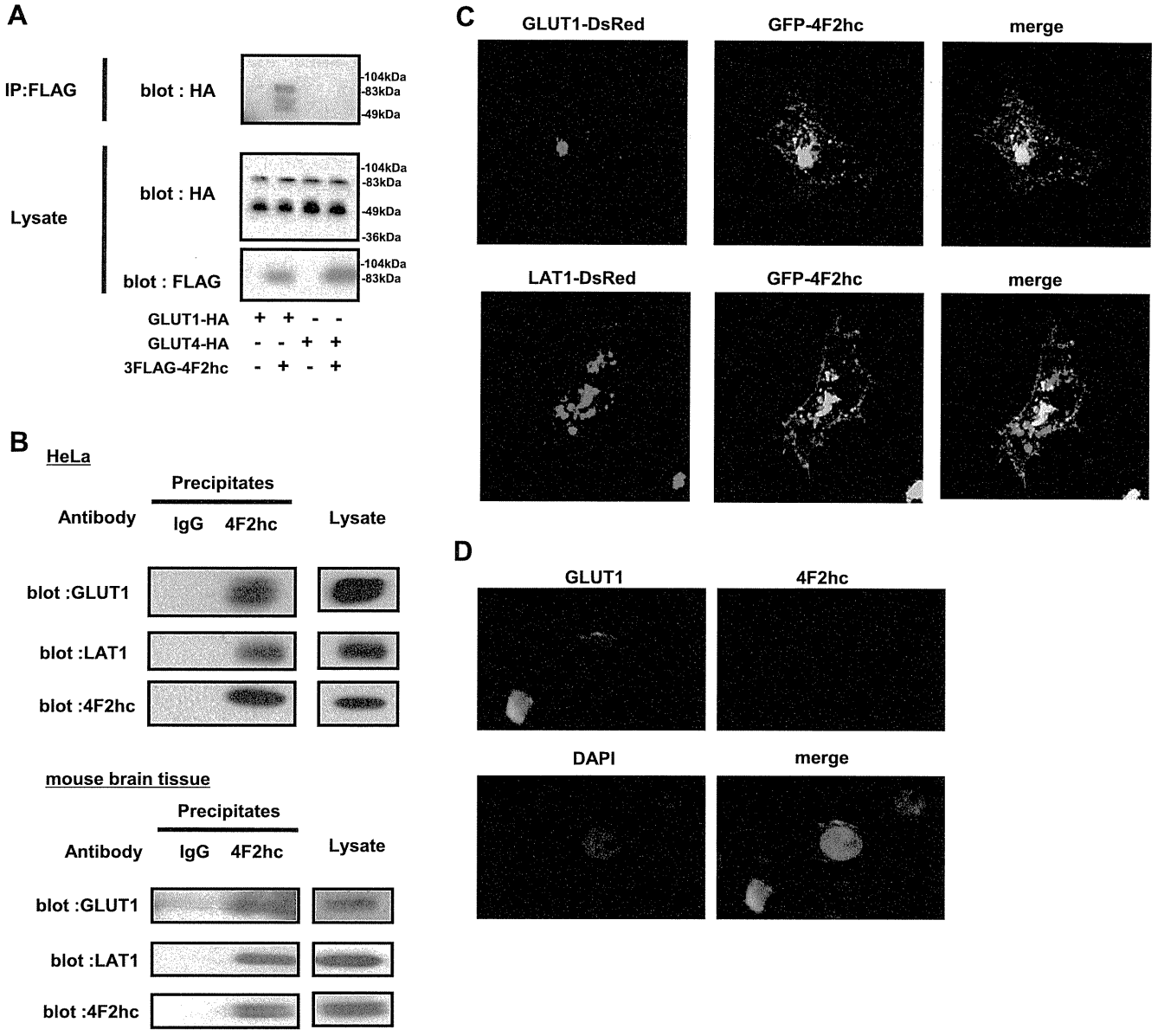

Fig. 2. 4F2hc associates with GLUT1 and shows colocalization with GLUT1. *A*: human embryonic kidney 293 (HEK293) cells were cotransfected with 3FLAG-4F2hc, GLUT1-hemagglutinin (HA), and GLUT4-HA expression plasmids. After 48 h, lysates were subjected to immunoprecipitation (IP) and immunoblotting. *B*: 4F2hc antibody was immobilized onto agarose beads (IPeX kit; Gene Bio-Application). The membrane fraction of HeLa cells (*top*) or mouse brain tissue (*bottom*) was added to the beads and immunoprecipitated. *C*: fluorescence images of HeLa cells cotransfected with green fluorescent protein (GFP)-4F2hc and either GLUT1-DsRed or LAT1-DsRed. *D*: immunostaining images, obtained using GLUT1 and CD98-specific antibodies in HeLa cells.

HA-tagged GLUT1 but not GLUT4 was detected in the FLAG-tagged 4F2hc immunoprecipitate. Next, we examined the association between endogenous GLUT1 and 4F2hc in HeLa cells and mouse brain, employing coimmunoprecipitation (Fig. 2*B*). GLUT1 was detected by the anti-4F2hc antibody, but not control IgG, in membrane fraction immunoprecipitates. The positive control, LAT1 in the anti-4F2hc antibody immunoprecipitate, was also confirmed in both HeLa cells and mouse brain.

Then, GFP-tagged 4F2hc and DsRed-tagged GLUT1 were transfected into HeLa cells, and colocalization of GLUT1 or LAT1 with 4F2hc was investigated. Considerable amounts of these GFP-tagged proteins appeared to be aggregated near nuclei and within intracellular vesicles, but LAT1 as well as GLUT1 apparently exhibited significant colocalization with 4F2hc at the plasma membrane and intracellular sites (Fig. 2*C*). In addition, endogenous GLUT1 and 4F2hc in HeLa cells were coimmunostained with anti-GLUT1 and anti-4F2hc antibodies (Fig. 2*D*). Although these staining data do not convincingly demonstrate an association between GLUT1 and 4F2hc, their colocalization at the plasma membrane raises this possibility.

Overexpression of 4F2hc increases glucose uptake. Since 4F2hc is likely to interact with GLUT1, the effect of 4F2hc on glucose transport activity was examined. 4F2hc reportedly regulates the functions of amino acid transporters, and increased 4F2hc expression enhances amino acid uptake. First, 4F2hc was overexpressed in HeLa cells, and the uptakes of 2-deoxyglucose and leucine were measured. Overexpression of

4F2hc increased glucose uptake in an expression level-dependent manner, by up to 55%, and leucine uptake was similarly increased (Fig. 3*B*). Interestingly, 4F2hc overexpression also increased the amount of GLUT1 protein (Fig. 3*A*). Since the transfection efficiency of the 4F2hc encoding plasmid in HepG2 cells was not sufficient, we employed adenovirus-mediated 4F2hc overexpression for HepG2 cells. Overexpression of 4F2hc by adenovirus in HepG2 cells also increased glucose uptake and the amount of GLUT1 protein (Fig. 3, *C* and *D*).

Knockdown of 4F2hc decreases glucose uptake and GLUT1 expression level. To further investigate the role of 4F2hc in glucose uptake, we performed loss of function analyses. Treatment with 4F2hc siRNA but not control siRNA reduced the 4F2hc protein expression level by ~90% (Fig. 4, *A* and *C*, *left*). Importantly, 4F2hc siRNA treatment also markedly reduced GLUT1 protein in both HeLa and HepG2 cells (*right* graphs of Fig. 4, *A* and *C*), with reduced glucose uptake (*left* graphs of Fig. 4, *B* and *D*). The altered transport activities of glucose caused by 4F2hc overexpression or siRNA treatment are generally very similar to those of leucine (*right* graphs of Fig. 3, *B* and *C*, and Fig. 4, *B* and *D*). To exclude the possibility of off-target effects of the siRNA knockdown experiments, we reintroduced a siRNA-resistant version of 4F2hc (siRNA is human; overexpressed 4F2hc is mouse). Reconstitution of mouse 4F2hc reversed the siRNA-mediated GLUT1 reduction (Supplemental Fig. S1*A*; Supplemental Material for this article is available online at the Journal website). In contrast, suppression of 4F2hc did not affect the expression of insulin Rβ (Supplemental Fig. S1*B*).

Enhanced green fluorescent protein (EGFP)-conjugated GLUT1 ligand, which has a receptor-binding domain in common with human T cell leukemia virus envelope glycoprotein, allows the amount of GLUT1 localized at the plasma membrane to be monitored by fluorescence staining (23, 24). Using this EGFP-conjugated ligand, we assessed the GLUT1 amount at the plasma membrane under conditions of either 4F2hc overexpression or knockdown in HeLa cells. The siRNA-mediated gene silencing of 4F2hc resulted in a reduction of the cell surface GLUT1 expression level, while 4F2hc overexpression produced an increase (Fig. 4*E*).

4F2hc is involved in GLUT1 stabilization and prevents GLUT1 from undergoing lysosomal degradation. To explore the mechanism underlying 4F2hc-related alterations in GLUT1 expression, we examined the mRNA levels of GLUT1 at 24 h and 48 h after the initiation of 4F2hc overexpression or 4F2hc siRNA transfection. Neither overexpression nor knockdown of 4F2hc significantly affected the mRNA levels of GLUT1 (Fig. 5, *A* and *B*). Since these observations indicate that 4F2hc does not regulate the transcriptional level of GLUT1, we considered the possibility that 4F2hc enhances GLUT1 stability and thereby increases glucose transport activity.

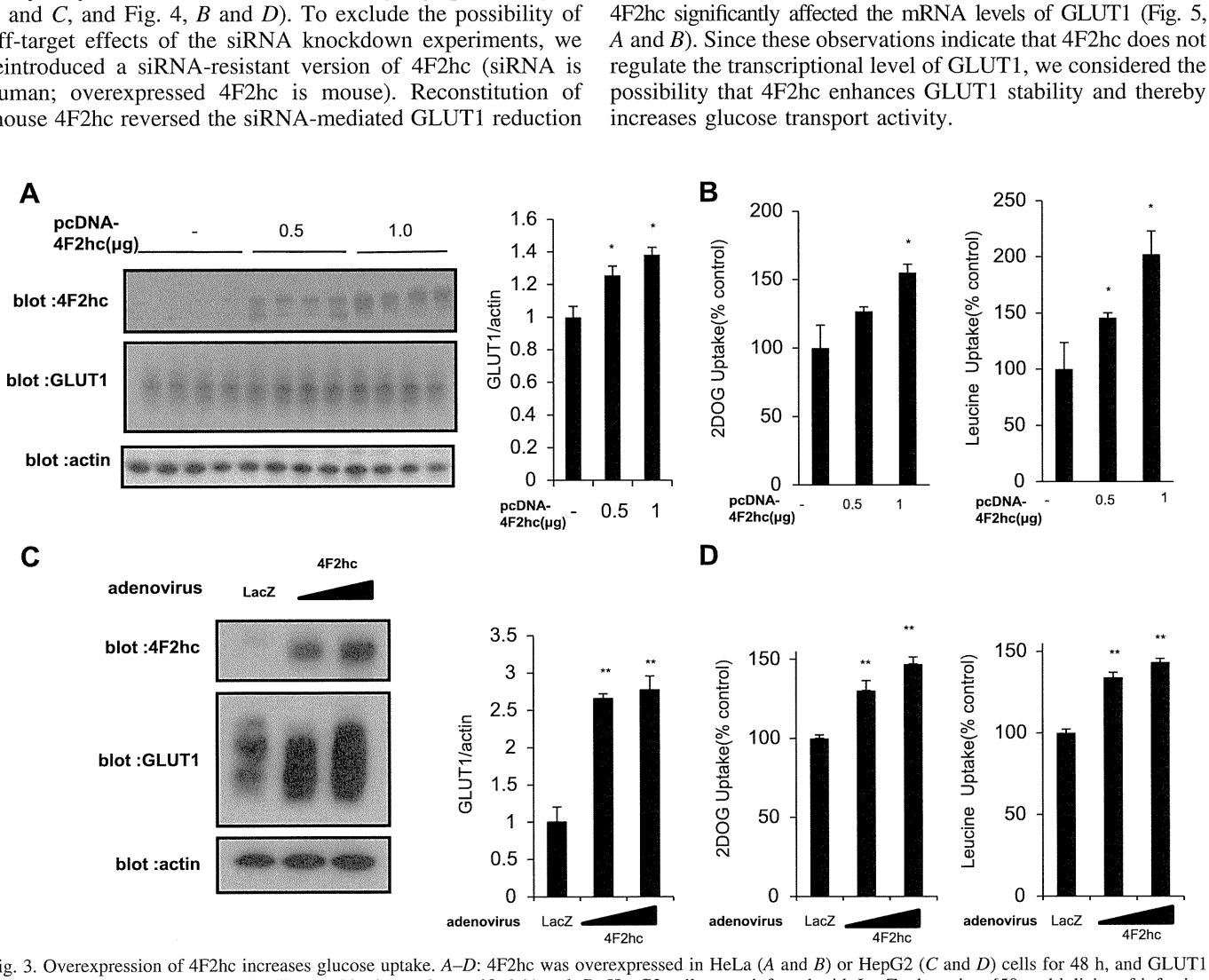

Fig. 3. Overexpression of 4F2hc increases glucose uptake. *A–D*: 4F2hc was overexpressed in HeLa (*A* and *B*) or HepG2 (*C* and *D*) cells for 48 h, and GLUT1 expression levels were measured by Western blotting and quantified (*A* and *C*). HepG2 cells were infected with LacZ adenovirus [50 multiplicity of infection (MOI)] or 4F2hc adenovirus (50 or 100 MOI). The uptakes of ^{3}H-2-deoxyglucose (2DOG; 5 min) and ^{14}C-leucine (1 min) were also measured (*B* and *D*). Data are expressed as means ± SE (n = 4). *$P < 0.05$; **$P < 0.01$, compared with controls.

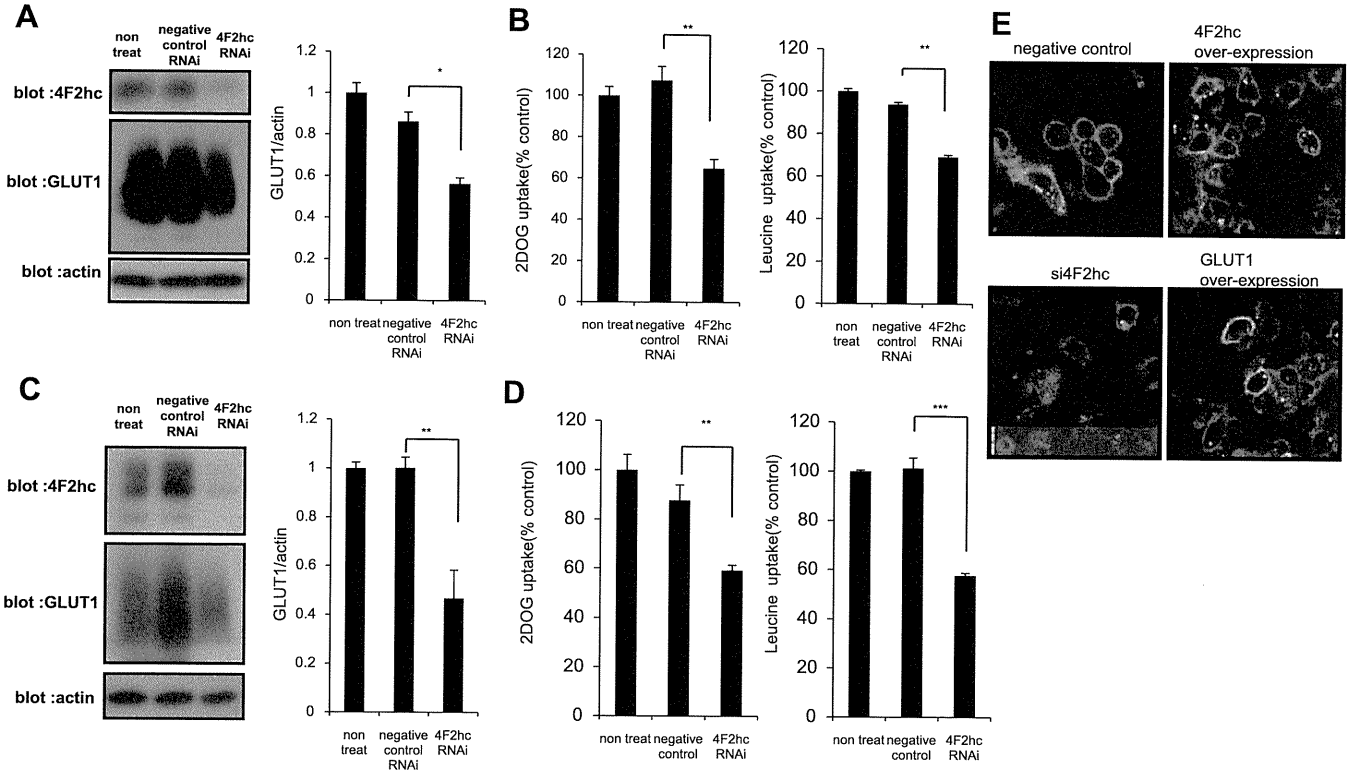

Fig. 4. Gene suppression of 4F2hc decreases glucose uptake. *A–D*: 4F2hc was suppressed in HeLa (*A* and *B*) and HepG2 (*C* and *D*) cells for 48 h, and GLUT1 expression levels were measured by Western blotting and quantified (*A* and *C*). The uptakes of ^{3}H-2-deoxyglucose (5 min) and ^{14}C-leucine (1 min) were also measured (*B* and *D*). *E*: 4F2hc or GLUT1 was overexpressed or small interfering RNA against 4F2hc (si4F2hc) was transfected into HeLa cells for 24 h. Enhanced GFP (EGFP)-conjugated GLUT1 ligand (AbCys, Paris, France) was added, and after a 30-min incubation, cell surface GLUT1 was observed by fluorescent microscopy. RNAi, RNA interference. Data are expressed as means ± SE ($n = 4$). $^{*}P < 0.05$; $^{**}P < 0.01$; $^{***}P < 0.001$, compared with negative controls.

The mechanism by which GLUT1 is degraded has not been elucidated in detail, but it has been shown that the lysosomal pathway contributes to GLUT1 degradation (30). GLUT1 degradation was investigated at the indicated period after addition of cycloheximide, an inhibitor of protein synthesis. Overexpression of 4F2hc significantly suppressed the GLUT1 degradation rate (Fig. 5*C*). On the other hand, the siRNA-mediated reduction in 4F2hc markedly increased the GLUT1 degradation rate, as compared with treatment with control siRNA (Fig. 5*D*). As previously reported, GLUT1 degradation was confirmed to be abolished by chloroquine, an agent suppressing lysosomal degradation (Fig. 5*E*) (32). In fact, it was shown that the proteasome blocker MG-132 did not stabilize GLUT1, which is consistent with previous reports (32). Taken together, our results strongly suggest that 4F2hc stabilizes GLUT1 by protecting it from lysosomal degradation.

DISCUSSION

In the present study, we newly demonstrated 4F2hc to be a protein interacting with GLUT1. 4F2hc, a membrane protein consisting of 529 amino acids and containing a single membrane-spanning domain, was initially identified as a lymphocyte activation antigen (13). 4F2hc reportedly forms a heterodimeric complex with specific light chain subunits of amino acid transporters such as LAT1 and LAT2 (14, 31, 33, 35). The heterodimer consisting of LAT1 or LAT2 and 4F2hc moves to the cell surface and exerts both neutral and basic amino acid transporter activity (25, 27). A previous study using deletion mutants revealed the domain of LAT1 indispensable for the association with 4F2hc to be the most NH_2-terminal transmembrane domain, and that a disulfide bridge connects their extracellular domains (5). A similar structure has been reported for the lactate transporter, which consists of 12 membrane-spanning monocarboxylate transporter 1 (MCT1) or MCT4 and a single membrane-spanning CD147 (20).

Given that GLUT1 has a similar structure, i.e., 12 putative membrane-spanning domains, similar to those of LAT1/2 and MCT1/4, we considered an association of 4F2hc with GLUT1 to be likely. We thus carried out experiments to assess this possibility. Indeed, the association between GLUT1 and 4F2hc was confirmed not only by coimmunoprecipitation of the overexpressed proteins, but also endogenously in HeLa cells and mouse brain, although it is unclear what percentage of GLUT1 is present as a heterodimer form with 4F2hc. While 4F2hc has a disulfide bridge between LAT1 with a cysteine on the extracellular side immediately after the transmembrane domain (5), this cysteine residue is not conserved in GLUT1, indicating that the association between GLUT1 and 4F2hc is not mediated by such a disulfide bond, but rather is simply noncovalent. Since the disulfide bridge connecting the extracellular domains of LAT1/2 and 4F2hc is not reportedly essential for association, the association between GLUT1 and 4F2hc without a disulfide bridge is not surprising (6, 27). However, in contrast to the essential role of 4F2hc in LAT1 or

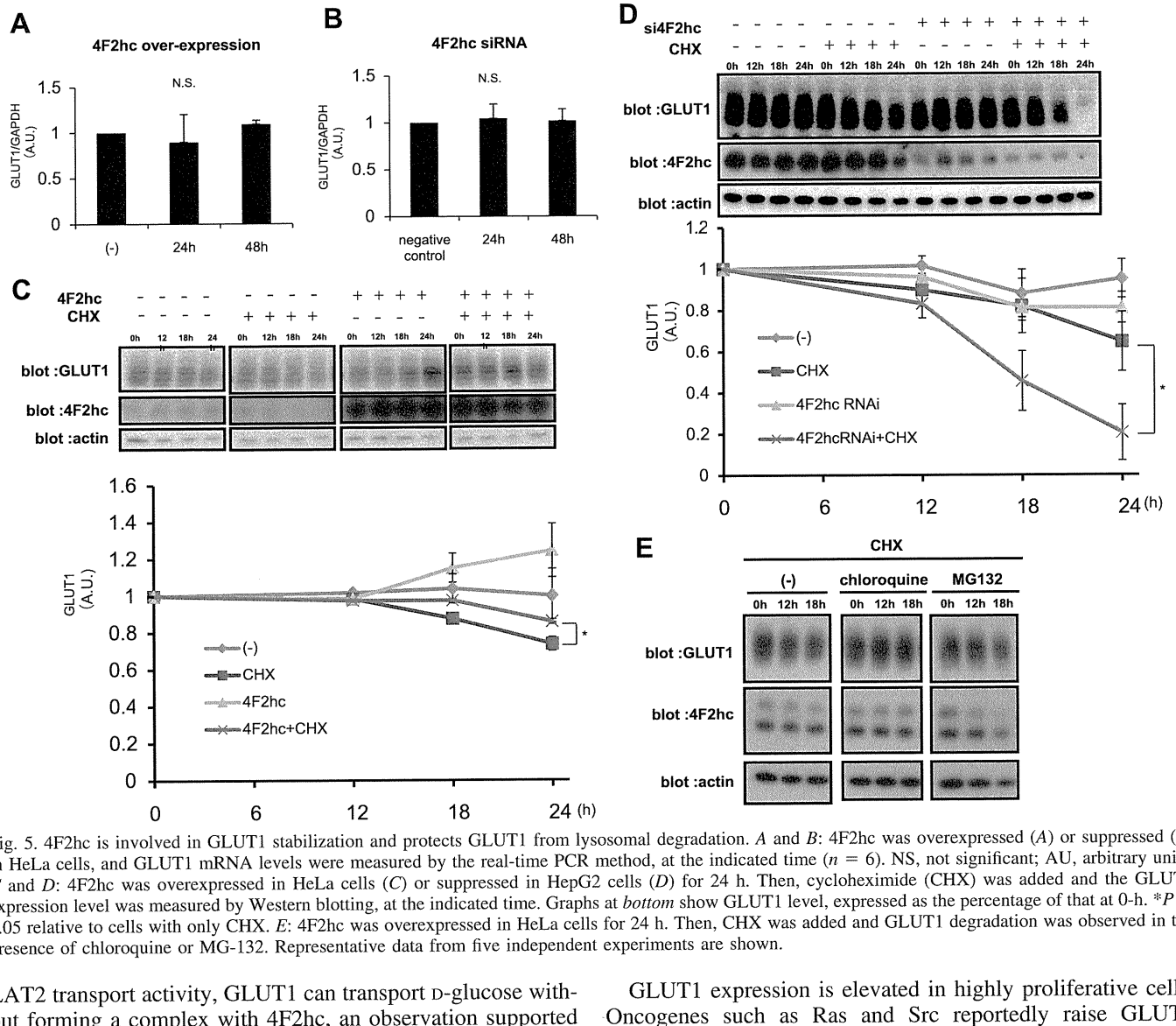

Fig. 5. 4F2hc is involved in GLUT1 stabilization and protects GLUT1 from lysosomal degradation. *A* and *B*: 4F2hc was overexpressed (*A*) or suppressed (*B*) in HeLa cells, and GLUT1 mRNA levels were measured by the real-time PCR method, at the indicated time ($n = 6$). NS, not significant; AU, arbitrary units. *C* and *D*: 4F2hc was overexpressed in HeLa cells (*C*) or suppressed in HepG2 cells (*D*) for 24 h. Then, cycloheximide (CHX) was added and the GLUT1 expression level was measured by Western blotting, at the indicated time. Graphs at *bottom* show GLUT1 level, expressed as the percentage of that at 0-h. $^*P < 0.05$ relative to cells with only CHX. *E*: 4F2hc was overexpressed in HeLa cells for 24 h. Then, CHX was added and GLUT1 degradation was observed in the presence of chloroquine or MG-132. Representative data from five independent experiments are shown.

LAT2 transport activity, GLUT1 can transport D-glucose without forming a complex with 4F2hc, an observation supported by previous reports showing the reconstitution of purified GLUT1 to an artificially constructed lectin membrane, as well as GLUT1 overexpression experiments in oocytes (15, 16, 17). Although we can speculate that heterodimeric complex formation with 4F2hc affects the kinetics of GLUT1 glucose transport activity to some degree, we were not able to clarify this issue herein because of difficulty measuring the percentages of GLUT1 alone and GLUT1/4F2hc forms.

On the other hand, it was clearly demonstrated that 4F2hc increases the amount of GLUT1 not only in whole cells but also at the plasma membrane. GLUT1 has been regarded as being involved in basal glucose uptake, and cells with high proliferative activity generally have high GLUT1 contents as shown in many cancers, fetal tissues, and the placenta (1, 22). We examined whether the 4F2hc expression level regulates not only amino acid transport activity via an association with LAT1, but also glucose transport activity via that with GLUT1. We found that 4F2hc overexpression increased not only leucine but also glucose uptake, while siRNA-mediated gene suppression of 4F2hc decreased these uptakes in HeLa and HepG2 cells (Figs. 3 and 4).

GLUT1 expression is elevated in highly proliferative cells. Oncogenes such as Ras and Src reportedly raise GLUT1 expression at the transcriptional level (4, 9). However, taking our results into consideration, the rate of GLUT1 degradation is also involved in regulation of the GLUT1 amount, and 4F2hc protects GLUT1 from lysosomal degradation. In addition, 4F2hc expression is also reportedly elevated in many cancers, suggesting its activity to correlate with cell proliferation and continuous growth (10, 19, 21, 28, 29). Thus, such growth-promoting stimuli not only increase GLUT1 synthesis at the transcriptional level, but also decrease the degradation of GLUT1 via upregulated 4F2hc. Previous reports described posttranscriptional modifications of GLUT1, such as monoubiquitinylation or sentrin conjugation, and their significance. These modifications reportedly regulate GLUT1 protein stability and cell function (7, 12). Thus, GLUT1 stability appears to also be important for determining both basal glucose uptake and cell proliferation. Taken together, these observations may support the hypothesis that increased expression of 4F2hc leads to an increased GLUT1 protein amount via suppression of GLUT1 degradation, resulting in the increased basal glucose uptake necessary for the progression of malignancy. In fact, the expression levels of both GLUT1 and 4F2hc are reportedly

elevated in many cancers and correlate with tumor progression (10, 28, 39). Further study is necessary to test our hypothesis.

In summary, our observations indicate that 4F2hc is likely to be involved in GLUT1 stabilization and to contribute to the regulation of not only amino acid but also glucose metabolism, both of which contribute to the incorporation of nutrients into highly proliferative cells. In this regard, the inhibition of 4F2hc may be regarded as a novel potential target for anticancer drugs.

ACKNOWLEDGMENTS

We thank Yoshikatsu Kanai for providing antibodies and the 3FLAG-4F2hc-expressing plasmid. This work was carried out with generous cooperation from the Research Center for Molecular Medicine, Hiroshima University.

DISCLOSURES

No conflicts of interest, financial or otherwise, are declared by the author(s).

REFERENCES

1. **Airley R, Mobasheri A.** Hypoxic regulation of glucose transport, anaerobic metabolism and angiogenesis in cancer: novel pathways and targets for anticancer therapeutics. *Chemotherapy* 53: 233–256, 2007.
2. **Asano T, Shibasaki Y, Ohno S, Taira H, Lin J, Kasuga M, Kanazawa Y, Akanuma Y, Takaku F, Oka Y.** Rabbit brain glucose transporter responds to insulin when expressed in insulin-sensitive Chinese hamster ovary cells. *J Biol Chem* 264: 3416–3420, 1989.
3. **Baer S, Casaubon L, Younes M.** Expression of the human erythrocyte glucose transporter Glut1 in cutaneous neoplasia. *J Am Acad Dermatol* 37: 575–577, 1997.
4. **Birnbaum M, Haspel H, Rosen O.** Transformation of rat fibroblasts by FSV rapidly increases glucose transporter gene transcription. *Science* 235: 1495–1498, 1987.
5. **Bröer S, Wagner C.** Structure-function relationships of heterodimeric amino acid transporters. *Cell Biochem Biophys* 36: 155–168, 2002.
6. **Fenczik C, Sethi T, Ramos J, Hughes P, Ginsberg M.** Complementation of dominant suppression implicates CD98 in integrin activation. *Nature* 390: 81–85, 1997.
7. **Fernandes R, Carvalho AL, Kumagai A, Seica R, Hosoya K, Terasaki T, Murta J, Pereira P, Faro C.** Downregulation of retinal GLUT1 in diabetes by ubiquitinylation. *Mol Vis* 10: 618–28, 2004.
8. **Fetchko M, Stagljar I.** Application of the split-ubiquitin membrane yeast two-hybrid system to investigate membrane protein interactions. *Methods* 32: 349–362, 2004.
9. **Flier J, Mueckler M, Usher P, Lodish H.** Elevated levels of glucose transport and transporter messenger RNA are induced by ras or src oncogenes. *Science* 235: 1492–1495, 1987.
10. **Fuchs B, Bode B.** Amino acid transporters ASCT2 and LAT1 in cancer: partners in crime? *Semin Cancer Biol* 15: 254–266, 2005.
11. **Ganapathy V, Thangaraju M, Prasad P.** Nutrient transporters in cancer: relevance to Warburg hypothesis and beyond. *Pharmacol Ther* 121: 29–40, 2009.
12. **Giorgino F, de Robertis O, Laviola L, Montrone C, Perrini S, McCowen KC, Smith RJ.** The sentrin-conjugating enzyme mUbc9 interacts with GLUT4 and GLUT1 glucose transporters and regulates transporter levels in skeletal muscle cells. *Proc Natl Acad Sci USA* 97: 1125–1130, 2000.
13. **Hemler M, Strominger J.** Characterization of antigen recognized by the monoclonal antibody (4F2): different molecular forms on human T and B lymphoblastoid cell lines. *J Immunol* 129: 623–628, 1982.
14. **Kanai Y, Segawa H, Miyamoto K, Uchino H, Takeda E, Endou H.** Expression cloning and characterization of a transporter for large neutral amino acids activated by the heavy chain of 4F2 antigen (CD98). *J Biol Chem* 273: 23629–23632, 1998.
15. **Kasahara M, Hinkle PC.** Reconstitution of D-glucose transport catalyzed by a protein fraction from human erythrocytes in sonicated liposomes. *Proc Natl Acad Sci USA* 73: 396–400, 1976.
16. **Kasahara M, Hinkle PC.** Reconstitution and purification of the D-glucose transporter from human erythrocytes. *J Biol Chem* 252: 7384–7390, 1977.
17. **Keller K, Strube M, Mueckler M.** Functional expression of the human HepG2 and rat adipocyte glucose transporters in *Xenopus* oocytes. Comparison of kinetic parameters. *J Biol Chem* 264: 18884–18889, 1989.
18. **Kim C, Cho S, Chun H, Lee S, Endou H, Kanai Y, Kim DK.** BCH, an inhibitor of system L amino acid transporters, induces apoptosis in cancer cells. *Biol Pharm Bull* 31: 1096–1100, 2008.
19. **Kim D, Kanai Y, Choi H, Tangtrongsup S, Chairoungdua A, Babu E, Tachampa K, Anzai N, Iribe Y, Endou H.** Characterization of the system L amino acid transporter in T24 human bladder carcinoma cells. *Biochim Biophys Acta* 1565: 112–121, 2002.
20. **Kirk P, Wilson M, Heddle C, Brown M, Barclay A, Halestrap A.** CD147 is tightly associated with lactate transporters MCT1 and MCT4 and facilitates their cell surface expression. *EMBO J* 19: 3896–3904, 2000.
21. **Kobayashi K, Ohnishi A, Promsuk J, Shimizu S, Kanai Y, Shiokawa Y, Nagane M.** Enhanced tumor growth elicited by L-type amino acid transporter 1 in human malignant glioma cells. *Neurosurgery* 62: 493–503, 2008.
22. **Macheda M, Rogers S, Best J.** Molecular and cellular regulation of glucose transporter (GLUT) proteins in cancer. *J Cell Physiol* 202: 654–662, 2005.
23. **Manel N, Battini J, Taylor N, Sitbon M.** HTLV-1 tropism and envelope receptor. *Oncogene* 24: 6016–6025, 2005.
24. **Manel N, Kim F, Kinet S, Taylor N, Sitbon M, Battini J.** The ubiquitous glucose transporter GLUT-1 is a receptor for HTLV. *Cell* 115: 449–459, 2003.
25. **Mastroberardino L, Spindler B, Pfeiffer R, Skelly P, Loffing J, Shoemaker C, Verrey F.** Amino-acid transport by heterodimers of 4F2hc/CD98 and members of a permease family. *Nature* 395: 288–291, 1998.
26. **Mueckler M, Caruso C, Baldwin S, Panico M, Blench I, Morris H, Allard W, Lienhard G, Lodish H.** Sequence and structure of a human glucose transporter. *Science* 229: 941–945, 1985.
27. **Nakamura E, Sato M, Yang H, Miyagawa F, Harasaki M, Tomita K, Matsuoka S, Noma A, Iwai K, Minato N.** 4F2 (CD98) heavy chain is associated covalently with an amino acid transporter and controls intracellular trafficking and membrane topology of 4F2 heterodimer. *J Biol Chem* 274: 3009–3016, 1999.
28. **Nawashiro H, Otani N, Shinomiya N, Fukui S, Nomura N, Yano A, Shima K, Matsuo H, Kanai Y.** The role of CD98 in astrocytic neoplasms. *Hum Cell* 15: 25–31, 2002.
29. **Ohkame H, Masuda H, Ishii Y, Kanai Y.** Expression of L-type amino acid transporter 1 (LAT1) and 4F2 heavy chain (4F2hc) in liver tumor lesions of rat models. *J Surg Oncol* 78: 265–271, 2001.
30. **Ortiz P, Honkanen R, Klingman D, Haspel H.** Regulation of the functional expression of hexose transporter GLUT-1 by glucose in murine fibroblasts: role of lysosomal degradation. *Biochemistry* 31: 5386–5393, 1992.
31. **Pineda M, Fernández E, Torrents D, Estévez R, López C, Camps M, Lloberas J, Zorzano A, Palacín M.** Identification of a membrane protein, LAT-2, that co-expresses with 4F2 heavy chain, an L-type amino acid transport activity with broad specificity for small and large zwitterionic amino acids. *J Biol Chem* 274: 19738–19744, 1999.
32. **Rosa SC, Gonçalves J, Judas F, Mobasheri A, Lopes C, Mendes AF.** Impaired glucose transporter-1 degradation and increased glucose transport and oxidative stress in response to high glucose in chondrocytes from osteoarthritic versus normal human cartilage. *Arthritis Res Ther* 11: R80, 2009.
33. **Rossier G, Meier C, Bauch C, Summa V, Sordat B, Verrey F, Kühn L.** LAT2, a new basolateral 4F2hc/CD98-associated amino acid transporter of kidney and intestine. *J Biol Chem* 274: 34948–34954, 1999.
34. **Sakoda H, Gotoh Y, Katagiri H, Kurokawa M, Ono H, Onishi Y, Anai M, Ogihara T, Fujishiro M, Fukushima Y, Abe M, Shojima N, Kikuchi M, Oka Y, Hirai H, Asano T.** Differing roles of Akt and serum- and glucocorticoid-regulated kinase in glucose metabolism, DNA synthesis, and oncogenic activity. *J Biol Chem* 278: 25802–25807, 2003.
35. **Segawa H, Fukasawa Y, Miyamoto K, Takeda E, Endou Kanai Y H.** Identification and functional characterization of a Na^+-independent neutral amino acid transporter with broad substrate selectivity. *J Biol Chem* 274: 19745–19751, 1999.
36. **Semenza G.** Targeting HIF-1 for cancer therapy. *Nat Rev Cancer* 3: 721–732, 2003.
37. **Smith T.** Facilitative glucose transporter expression in human cancer tissue. *Br J Biomed Sci* 56: 285–292, 1999.
38. **Stagljar I, Korostensky C, Johnsson N, te Heesen S.** A genetic system based on split-ubiquitin for the analysis of interactions between membrane proteins in vivo. *Proc Natl Acad Sci USA* 95: 5187–5192, 1998.
39. **Younes M, Brown RW, Stephenson M, Gondo M, Cagle PT.** Overexpression of Glut1 and Glut3 in stage I non-small cell lung carcinoma is associated with poor survival. *Cancer* 80: 1046–1051, 1997.

Human Molecular Genetics, 2011, Vol. 20, No. 7 **1274–1284**
doi:10.1093/hmg/ddq568
Advance Access published on January 3, 2011

Wolfram syndrome 1 gene (*WFS1*) product localizes to secretory granules and determines granule acidification in pancreatic β-cells

Masayuki Hatanaka[1,2], Katsuya Tanabe[1], Akie Yanai[3], Yasuharu Ohta[1], Manabu Kondo[1], Masaru Akiyama[1], Koh Shinoda[3], Yoshitomo Oka[4] and Yukio Tanizawa[1,*]

[1]Division of Endocrinology, Metabolism, Hematological Sciences and Therapeutics, Department of Bio-Signal Analysis, [2]Department of Diabetes Research and [3]Division of Neuroanatomy, Department of Neuroscience, Yamaguchi University Graduate School of Medicine, Ube, Yamaguchi, Japan and [4]Division of Molecular Metabolism and Diabetes, Tohoku University Graduate School of Medicine, Sendai, Miyagi, Japan

Received October 15, 2010; Revised and Accepted December 29, 2010

Wolfram syndrome is an autosomal recessive disorder characterized by juvenile-onset insulin-dependent diabetes mellitus and optic atrophy. The gene responsible for the syndrome (*WFS1*) encodes an endoplasmic reticulum (ER) resident transmembrane protein. The *Wfs1*-null mouse exhibits progressive insulin deficiency causing diabetes. Previous work suggested that the function of the WFS1 protein is connected to unfolded protein response and to intracellular Ca^{2+} homeostasis. However, its precise molecular function in pancreatic β-cells remains elusive. In our present study, immunofluorescent and electron-microscopic analyses revealed that WFS1 localizes not only to ER but also to secretory granules in pancreatic β-cells. Intragranular acidification was assessed by measuring intracellular fluorescence intensity raised by the acidotrophic agent, 3-[2,4-dinitroanilino]-3′-amino-*N*-methyldipropyramine. Compared with wild-type β-cells, there was a 32% reduction in the intensity in WFS1-deficient β-cells, indicating the impairment of granular acidification. This phenotype may, at least partly, account for the evidence that *Wfs1*-null islets have impaired proinsulin processing, resulting in an increased circulating proinsulin level. Morphometric analysis using electron microscopy evidenced that the density of secretory granules attached to the plasma membrane was significantly reduced in *Wfs1*-null β-cells relative to that in wild-type β-cells. This may be relevant to the recent finding that granular acidification is required for the priming of secretory granules preceding exocytosis and may partly explain the fact that glucose-induced insulin secretion is profoundly impaired in young prediabetic *Wfs1*-null mice. These results thus provide new insights into the molecular mechanisms of β-cell dysfunction in patients with Wolfram syndrome.

INTRODUCTION

Diabetes mellitus is a heterogeneous disorder characterized by glucose intolerance that affects over 170 million people worldwide (1). The disease arises from a combination of absolute (type 1) or relative (type 2) insulin deficiency with variable peripheral insulin resistance. The failure of insulin supply is implicated to result from both impaired β-cell function and decreased β-cell mass (2–4).

Wolfram syndrome (OMIM 222300) is an autosomal recessive disorder with severe neurodegeneration. Affected individuals present with juvenile-onset insulin-dependent diabetes mellitus and optic atrophy (5). Postmortem studies of the pancreas from patients with Wolfram syndrome have revealed a selective β-cell loss (6). The gene responsible for the disorder, *WFS1*, encodes a novel transmembrane protein (7,8). The WFS1 protein, also called Wolframin, consists of 890 amino acids and is predicted to have nine membrane-spanning

*To whom correspondence should be addressed at: Division of Endocrinology, Metabolism, Hematological Sciences and Therapeutics, Yamaguchi University Graduate School of Medicine, 1-1-1 Minamikogushi, Ube, Yamaguchi 755-8505, Japan. Tel: +81 836222250; Fax: +81 836222342; Email: tanizawa@yamaguchi-u.ac.jp

domains. This protein is known to be embedded in the endoplasmic reticulum (ER) membrane (9). Mice with a disrupted *Wfs1* gene exhibit a selective β-cell loss. This phenotype has been thought to result from the activation of ER stress, impaired cell cycle progression and apoptosis (10–14). In addition, insulin secretion from the isolated islets of *Wfs1*-null mice was shown to be impaired (15). An early study has shown that WFS1 might serve directly as a divalent ion channel or, alternatively, as a regulator of existing channel activity (16). Later, it was demonstrated that WFS1 positively modulates the Ca^{2+} level in ER by increasing the rate of Ca^{2+} uptake (10). However, the lack of distinct domains in WFS1 makes it difficult to understand its precise physiological function in pancreatic β-cells.

Secretory granules are acidified through a proton gradient, established and maintained by coordinated action between H^+-pumping vacuolar-type ATPase (V-ATPase) (17) and ClC-3, a chloride ion channel (18). The low pH of late secretory granules is necessary for proinsulin processing, and in addition, for the priming of the granules preceding exocytosis (18).

In this study, WFS1 was found to localize not only in ER but also in dense-core secretory granules in pancreatic β-cells. *Wfs1*-null mice exhibited severely impaired insulin secretion in response to glucose. These observations prompted us to investigate the functional significance of the granule-resident WFS1 protein, including its role in the acidification of insulin secretory granules, as an additional physiological function of WFS1.

RESULTS

WFS1 protein localizes to insulin secretory granules

Previous studies have shown that the majority of WFS1-immunoreactive cells were insulin-producing β-cells (16,19) in pancreatic islets. However, the precise intracellular localization of WFS1 in β-cells has not been examined, whereas this protein is thought to localize predominantly in ER in WFS1-overexpressing heterologous cells (7,9,11,20). We thus attempted to detail its intracellular localization to obtain a clue to understand further physiological roles of WFS1 in pancreatic β-cells. Immunohistochemical analysis of pancreatic sections from wild-type (*Wt*) animals using anti-WFS1 antibodies and antibodies against markers for either ER or secretory granules was performed. As shown in Figure 1A–C, only a little part of the immunoreactive area for WFS1 protein (red) appeared to merge with that for Grp78, an ER marker (green). Surprisingly, there appeared to be better co-localization of WFS1 protein with chromogranin A (green), a marker of secretory granules (Fig. 1D–F). To further substantiate the localization of WFS1 protein to the secretory granule, immunoelectron microscopy using anti-WFS1 antibodies was performed. β-Cells could be distinguished from α- and δ-cells by the appearance of the secretory granules. β-Cell granules have a white halo, which is not apparent in α- and δ-granules. As described previously (19), immunoreactivity for WFS1 protein was observed in β-cells but not in α-cells (Fig. 1G). As shown in Figure 1H, there appeared to be the accumulation of immunoreactivity not only in ER but also in dense-core granules in *Wt* β-cells. High magnification more clearly showed accumulation of immunoreactivity in the periphery of electron-dense-core granules accompanied by a halo in *Wt* β-cells (Fig. 1I). Consistently, no immunoreactivity for WFS1 was observed in WFS1-deficient β-cells (Fig. 1J). These results clearly demonstrate that WFS1 localizes not only in ER but also in secretory granules in pancreatic β-cells. The intracellular distribution of WFS1 in pancreatic β-cells was assessed by immunogold electron microscopic analysis (Fig. 1K–M). We quantified the labeling by counting gold particles per β-cell area and found ~40% more immunogold particles in secretory granules relative to those in ER (Fig. 1M). No particles were found in mitochondria. From these immunohistological observations at the tissue and ultrastructural levels, we concluded that WFS1 preferentially localizes in dense-core granules in pancreatic β-cells.

WFS1 deficiency impairs intragranular acidification

Of interest to the function of WFS1, despite a lack of distinct domains in WFS1, it has nine membrane-spanning domains, enabling us to expect that this protein may function as an ion-channel regulator. We hypothesized that WFS1 in insulin granules might play a role in the regulation of acidification of insulin granules. To test this hypothesis, granular acidification was examined by incubating mechanically dispersed islet cells with the acidotrophic agent 3-[2,4-dinitroanilino]-3′-amino-*N*-methyldipropyramine (DAMP) (21,22). Insulin-producing cells were selected by co-staining for insulin. Indirect immunofluorescence intensity, raised by DAMP accumulation, in the whole cell with the exception of the nucleus was measured. The number of lysosomes in β-cells is negligible compared with insulin granules (estimated as 48 and 11 000 per β-cell, respectively) (17) and, therefore, will not significantly contribute to the fluorescent signal. Indirect immunofluorescence intensity for DAMP (green) in insulin immunoreactive cells from *Wfs1*$^{-/-}$ mice appeared to be weaker than that in insulin immunoreactive cells from *Wt* mice (Fig. 2A–I). *Wfs1*$^{-/-}$ β-cells had significantly reduced immunofluorescence intensity to an average of 68% of the average intensity of *Wt* β-cells (Fig. 2J). *Wt* β-cells incubated with bafilomycin A1, a V-ATPase inhibitor, exhibited an even larger reduction in intensity. These observations were replicated when granular acidification was assessed using LysoTracker, another acidotrophic probe (Fig. 2K). Hence, these results strongly suggest that WFS1 plays a role in maintenance of acidification in dense-core granules of pancreatic β-cells.

Islets from WFS1-deficient mice have impaired insulin processing

Processing of proinsulin into mature insulin requires cleavage by the prohormone convertase enzymes, PC1/3 and PC2 (23–25). These enzymes have an acidic optimum pH (23), and the conversion of proinsulin to insulin is strictly dependent on a low pH (24,26). We thus hypothesized that proinsulin conversion to insulin might be affected by impaired intragranular acidification in WFS1-deficient β-cells. To test this hypothesis, the amounts of insulin and proinsulin in isolated islets

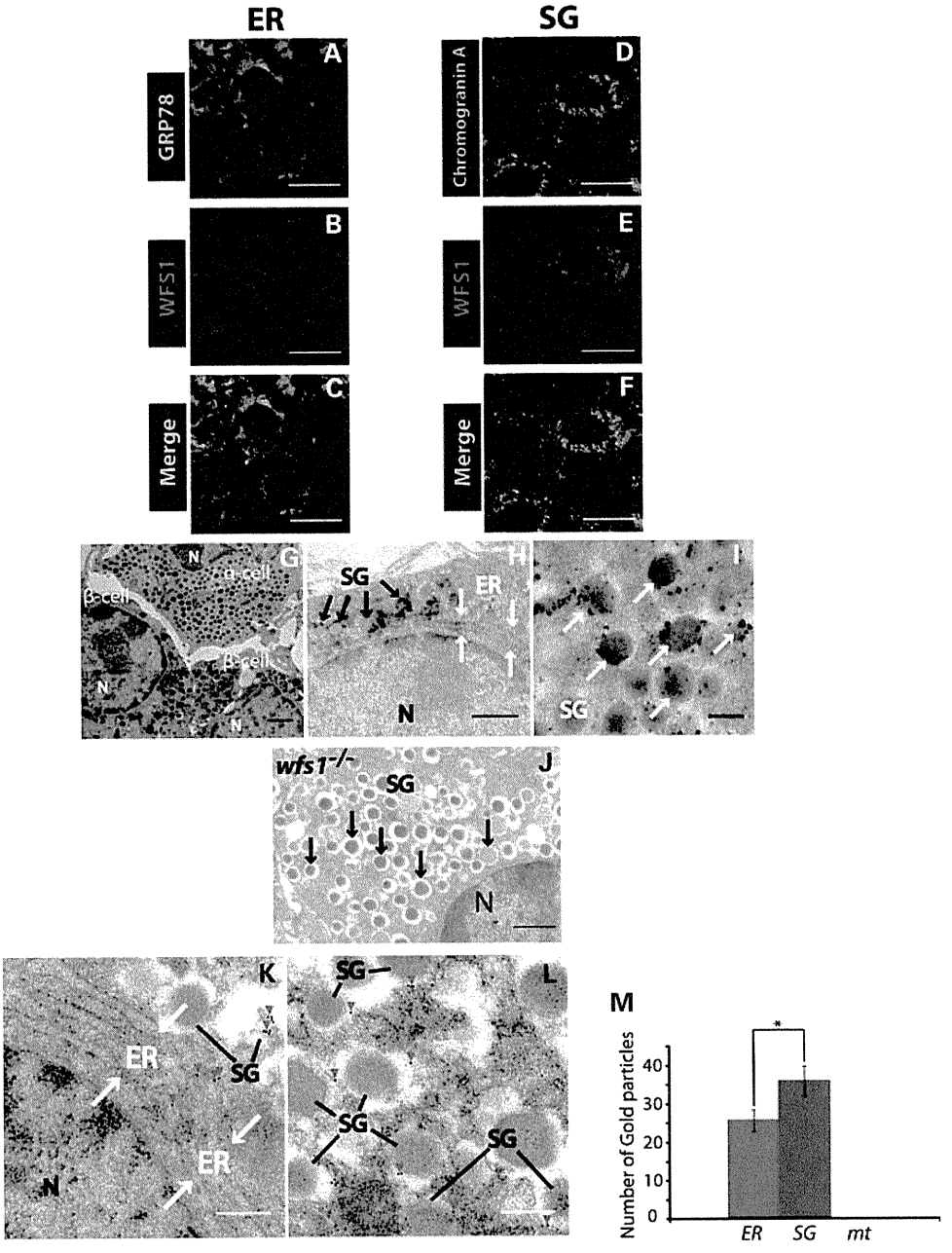

Figure 1. Localization of WFS1 to secretory granules (SG) in pancreatic β-cells. (**A**–**F**) Immunofluorescence analysis of pancreatic islets of *Wt* mice using antibodies to WFS1 (B and E, red) and antibodies to either GRP78 (A, green) or chromogranin A (D, green). Scale bars represent 10 μm. Immunoelectron microscopy of WFS1 with the DAB method, performed on pancreatic sections from $Wfs1^{-/-}$ and *Wt* mice (**G**–**J**). (G) Representative electron micrograph showing the localization of WFS1 in β-cells but not in α-cells. Scale bar represents 1 μm. Red arrow heads indicate WFS1 immunoreactivity. (H) Representative areas of β-cell from *Wt* mice. Scale bars represent 500 nm. (I) High magnification of representative dense-core secretory granules in β-cell from *Wt* mice. Scale bar represents 200 nm. (J) Representative area of β-cell from $Wfs1^{-/-}$ mice. Scale bars represent 500 nm. (**K** and **L**) Distribution of WFS1 in pancreatic β-cells. The distribution of WFS1 is shown by immunogold labeling (red arrow heads indicate examples). Bar: 200 nm. (**M**) Gold particle frequency in ER and SG per β-cell area (36 μm^2 × 24 sections). SG, secretory granule; ER, endoplasmic reticulum; mt, mitochondria.

from mice at 12 weeks of age were examined by western blot. As shown in Fig. 3A, there was a significant reduction in the abundance of mature insulin relative to GAPDH, a control for protein loading, in $Wfs1^{-/-}$ islets compared with that in *Wt* mice (Fig. 3B), whereas the proinsulin level was not altered (Fig. 3C). There was a consistent parallel increase in the proinsulin to insulin ratio in $Wfs1^{-/-}$ islets relative to that in *Wt* islets (Fig. 3D), indicating that the lack of WFS1 causes impaired insulin processing. In accordance with this observation, the plasma proinsulin level after 6 h fasting was higher in WFS1-deficient mice than in *Wt* mice (Table 1). Expression levels of prohormone convertases were further examined. As shown in Figure 3E, there was a significant reduction in the PC1/3 level in $Wfs1^{-/-}$ islets relative to

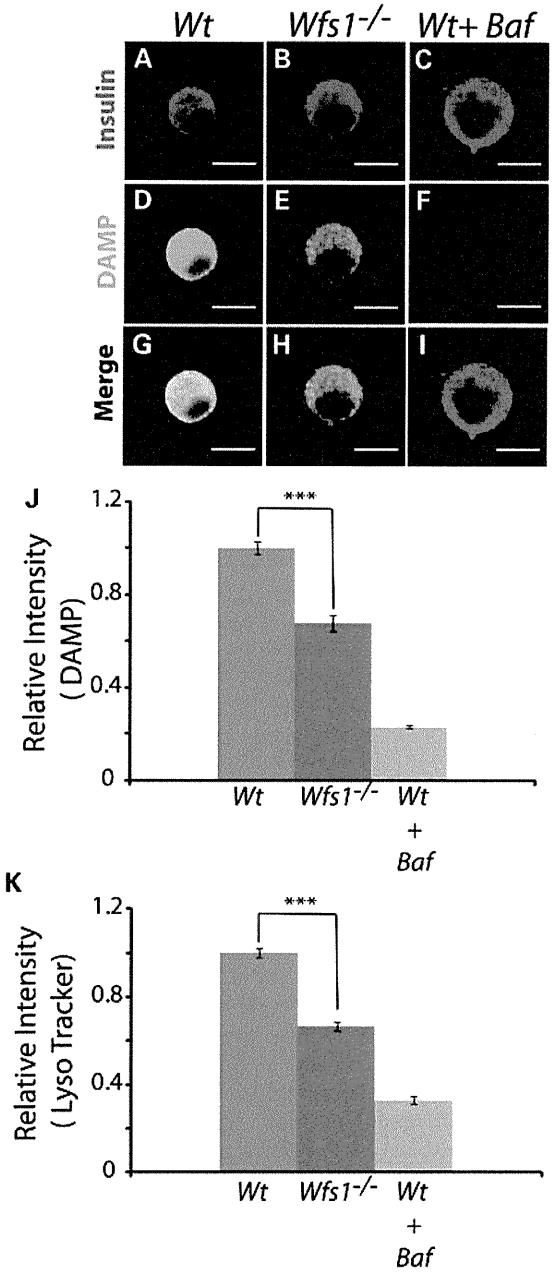

Figure 2. Disturbed intragranular acidification in WFS1-deficient β-cells. Dispersed islet cells from *Wfs1*$^{-/-}$ and *Wt* mice were incubated with either 3 μM DAMP or 25 nM LysoTracker for 1 h or 30 min, respectively, and were then fixed. (**A–I**) Representative photographs of DAMP-incubated islet cells stained with antibodies to DNP (green) and insulin (red). Treatment of *Wt* islet cells with bafilomycin A1 was a control of disturbed intragranular acidification. (**J**) Mean fluorescence intensity of DNP per area of each insulin-immunoreactive cell was measured. The results were obtained from 76 randomly selected *Wfs1*$^{-/-}$ β-cells and 65 *Wt* β-cells from nine different animals of each genotype. Relative intensity was expressed as the mean ± SEM. ***$P < 0.001$. (**K**) Relative mean fluorescence intensity of LysoTracker per area of each insulin-immunoreactive cell was calculated in a total of 167 *Wt* β-cells and 170 *Wfs1*$^{-/-}$ β-cells from six different animals of each genotype and graphically expressed as the mean ± SEM. ***$P < 0.001$.

that in *Wt* islets, whereas the PC2 level was not altered (Fig. 3F and G). In *Wfs1* haploinsufficiency (*Wfs1*$^{+/-}$) islets, no appreciable changes were observed in either proinsulin processing or PC1/3 expression (data not shown). To further examine the mechanism linking the lack of WFS1 to the reduced PC1/3 level, immunoprecipitation analysis using anti-WFS1 antibody was performed. However, a direct interaction of WFS1 with PC1/3 was not proved (data not shown).

WFS1 plays a role in regulation of insulin secretion *in vivo*

It has been documented that islets isolated from *Wfs1*$^{-/-}$ mice exhibited a decrease in insulin secretion in response to glucose (15). We further examined the effect of lack of WFS1 on *in vivo* insulin secretion in response to glucose at 12 weeks of age. At this age, the non-fasting blood glucose level of *Wfs1*$^{-/-}$ mice was similar to that of *Wt* mice (Fig. 4A). Glucose tolerance tests were then conducted. Blood glucose levels after overnight fasting were indistinguishable between the mutant mice and the *Wt* mice. The blood glucose level at 60 min after intraperitoneal glucose injection in WFS1-deficient mice was slightly but significantly increased relative to that in *Wt* mice (Fig. 4B). Insulin secretory response to glucose was then assessed. Whereas there was no significant change in the insulin level after overnight fasting, serum insulin levels at 2 and 15 min after glucose challenge were markedly reduced in *Wfs1*$^{-/-}$ mice compared with those in *Wt* mice. The reduced insulin levels in *Wfs1*$^{-/-}$ mice persisted until 30 min after glucose injection (Fig. 4C).

The effect of WFS1 deficiency on the β-cell mass at this age was examined. As shown in Figure 4D, insulin-positive cells still appeared to be maintained in 12-week-old WFS1-deficient mice. The insulin-immunoreactive area in WFS1-deficient mice was indistinguishable from that in *Wt* mice (Fig. 4E). Consistently, whole pancreatic insulin content was maintained in WFS1-deficient mice compared with that in *Wt* mice (Fig. 4F). These results indicate that WFS1-deficient mice have severely impaired insulin secretion in response to glucose, when abundance of β-cells is still maintained, before progressive β-cell loss becomes apparent.

WFS1 deficiency results in reduction in plasma membrane-attached secretory granules in pancreatic β-cells

To further examine the effects of WFS1 deficiency, the morphological characteristics of dense-core granules were studied by an electron microscopic analysis of pancreatic sections from randomly fed 12-week-old mice. There were no apparent differences in the appearance of electron-dense-core granules between *Wfs1*-null and *Wt* β-cells, whereas mild dilatation of ER was shown in some WFS1-deficient β-cells, as described previously (11,14) (Fig. 5A). There was no significant difference in granule size assessed by measuring granule diameter (Fig. 5B). Granule density (granule number per cytosolic area) was not affected in WFS1-deficient β-cells (Fig. 5C), either. On the other hand, the density of insulin granules docking to the plasma membrane appeared to be decreased. In fact, the number of insulin granules directly attached to the plasma membrane per cytosolic area (Fig. 5E) and per granule density (Fig. 5F) was significantly reduced in *Wfs1*$^{-/-}$ β-cells compared with that in *Wt*

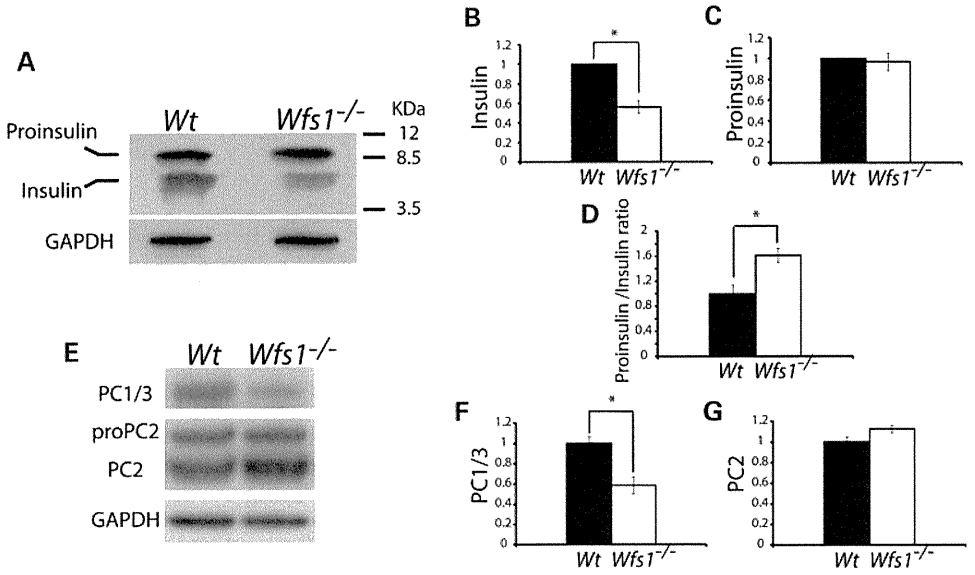

Figure 3. Impaired insulin processing in WFS1-deficient β-cells. Islets were isolated from 12-week-old *Wfs1*$^{-/-}$ and *Wt* mice. (**A**) Western blot analysis with antibodies to insulin and GAPDH. Representative results of multiple independent experiments are presented. Densities of mature insulin and proinsulin were measured and normalized to GAPDH. The results for insulin versus GAPDH (**B**), proinsulin versus GAPDH (**C**) and relative proinsulin/insulin ratio (**D**) are graphically illustrated as the mean ± SEM. $^{*}P < 0.05$. (**E**) Western blot analysis with anti-PC1, anti-PC2 and anti-GAPDH antibodies. Representative results from four independent experiments are presented. (**F** and **G**) Densities of PC1 and PC2 were measured and normalized to GAPDH. Mean protein levels ± SEM are summarized in the graph. $^{*}P < 0.05$.

β-cells. These results suggest that WFS1 function somehow determines the intracellular distribution of secretory granules, especially the docking of insulin granules to the plasma membrane. This defect may underlie, at least in part, the impairment of glucose-stimulated insulin secretion and hence may play a role in the regulation of the insulin secretory pathway.

DISCUSSION

The combination of β-cell dysfunction and β-cell loss results in progressive insulin deficiency in *Wfs1*-null mice. WFS1 has been thought to be connected with unfolded protein response and intracellular Ca^{2+} homeostasis. The present study provides additional insights into the physiological role of WFS1 in pancreatic β-cells. The following observations were documented: (i) WFS1 protein localizes in secretory granules in pancreatic β-cells; (ii) lack of WFS1 results in disturbed intragranular acidification; (iii) WFS1 deficiency causes impaired conversion of proinsulin to insulin accompanied by a decreased PC1/3 protein level; (4) WFS1-deficient β-cells have a reduced number of dense-core vesicles attached to the plasma membrane, possibly providing cellular evidence correlated with impaired insulin secretion. Taken together, these findings provide additional insights into the mechanisms of β-cell dysfunction in Wolfram syndrome.

In our present study, histological analysis at the tissue level and the ultrastructural level revealed that WFS1 was expressed not only in ER but also in dense-core granules in mouse pancreatic β-cells. In addition, immunogold particles against WFS1 were detected rather more abundantly in dense-core granules than in ER, indicating that WFS1 in dense-core granules as well as in ER could be required for sufficient β-cell function. In this regard, WFS1-deficient β-cells exhibited disturbed intragranular acidification. Because a number of membrane proteins in dense-core granules participate in important processes, such as vesicle trafficking or generation of intragranular acidification, impaired intragranular acidification is likely to result from the defect of WFS1 in dense-core granules. Intragranular acidification depends on the simultaneous operation of the V-type H^{+}-ATPase and the ClC-3 Cl^{-} channel on the insulin granule membrane (18). Although the present study did not address how WFS1 contributes to the maintenance of intragranular acidification, the function of WFS1 in insulin granules could be connected with the regulation of these channel activities.

Impaired proinsulin processing was documented in WFS1-deficient islets. Granted the impaired vesicular acidification, this is an expected and confirmatory result because acidic pH in insulin granules is required for sufficient endopeptidase activities of PC1/3 and PC2, and hence efficient proinsulin processing (23). In addition, we observed that the PC1/3 level but not the PC2 level was decreased in WFS1-deficient islets. The reduced PC1/3 level may contribute to a further reduction in endopeptidase activity of PC1/3. However, a direct link between lack of WFS1 and reduced PC1/3 level has not been proved. Exact mechanisms by which WFS1 deficiency causes reduced PC1/3 levels are unclear at this stage. Both PC1/3 and PC2 are expressed in the β-cells, whereas only PC2 is predominantly expressed in α-cells (27). If β-cells were selectively lost, decrease in PC1/3 protein would be apparent compared with PC2 in total islets. However, this is not the case because β-cell mass is not decreased at this age (Fig. 4D–F).

Secretory granules in β-cells can be divided into the readily releasable pool (RRP) and the reserve pool (28–30). The process in which granules proceed from the reserve pool

Table 1. Serum insulin and proinsulin level of 12–16-week-old mice after a 6 h fast

Genotype	Blood glucose (mg/dl)	Serum insulin (ng/ml)	Serum proinsulin (ng/ml)	Proinsulin/insulin (%)	Number
Wt	185 (±9)	0.34 (±0.03)	0.026 (±0.005)	4.6 (±0.8)	9
Wfs1$^{-/-}$	182 (±11)	0.47 (±0.05)	0.050 (±0.006)*	7.0 (±1.0)	9

*$P < 0.01$ by one-factor Student's *t*-test compared with *wt* mice.

into the RRP is referred to as mobilization and involves priming by ATP hydrolysis. A recent study demonstrated that acidification of the secretory granules is necessary for the priming of the granules preceding excytosis (18,22,31,32). We observed that the number of dense-core granules attached to the plasma membrane was reduced in β-cells of *Wfs1*-null mice, in association with impaired granular acidification. Docking and priming precede the Ca^{2+}-evoked exocytic granular fusion events, and thus this observation may explain, at least in part, the impaired glucose-stimulated insulin secretion, another pathologic feature of β-cells, in *Wfs1*-null mice.

What is the molecular function of WFS1 protein? Current information on this fundamental question is very limited. As mentioned earlier, WFS1 protein may be a channel/transporter or its functional regulator (10,16). Calcium, protons or chloride channels are candidates in ER and in the insulin secretory granules for regulation of ER calcium homeostasis or secretory granule acidification. It was also reported that WFS1 protein bound to the sodium–potassium ATPase b1 subunit (33) and calmodulin (34), although the functional significance of binding to these target molecules is unknown. Very recently, WFS1 was reported to negatively regulate activating transcription factor 6α through the ubiquitin–proteasome pathway (35). According to this finding, WFS1 may regulate target protein function, by modulating their turnover. Clearly, WFS1 can regulate multiple cellular functions and play a different role in each compartment in pancreatic β-cells.

In conclusion, previous studies have shown that WFS1 is an ER transmembrane protein that is implicated in cellular Ca^{2+} homeostasis and unfolded protein response in β-cells. Our present study has demonstrated that the WFS1 protein is also localized to the secretory granules in mouse pancreatic β-cells and suggested its functional significance. The current study provides new insights into WFS1 protein function and the pathophysiology of Wolfram syndrome.

MATERIALS AND METHODS

Animal production and metabolic phenotype analysis

Generation and genotyping of *Wfs1*$^{-/-}$ mice have been described previously (15). We maintained *Wfs1*$^{-/-}$ mice on a C57BL/6J background. For the glucose tolerance test, mice were subjected to overnight fasting followed by intraperitoneal glucose injection (2.0 g/kg). Blood glucose was measured at 0, 15, 30 and 60 min after injection using an automatic blood glucose meter, Antsense III (Horiba, Kyoto Japan). Blood samples were collected at 0, 2, 5, 15 and 30 min after injection. Insulin levels were measured by an enzyme-linked immunosorbent assay (ELISA) kit using a rat insulin standard (Morinaga, Yokohama, Japan) or the mouse insulin ELISA kit (ALPCO, Salem, NH, USA). Proinsulin was measured by the mouse proinsulin ELISA kit (ALPCO). All the experiments were carried out in male mice and were approved by the Animal Ethics Committee of Yamaguchi University School of Medicine.

Immunofluorescent staining of pancreatic islets

Pancreata were isolated from 12-week-old *Wfs1*$^{-/-}$ mice. Isolated pancreata were fixed overnight in 4% paraformaldehyde at room temperature. Tissue was then routinely processed for paraffin embedding, and 3-μm sections were cut and mounted on glass slides. The sections were immunostained with antibodies to insulin (Dako Cytomation, CA, USA), Glucagon (Santa Cruz, CA, USA), GRP78 (BD Biosciences, San Jose, CA, USA) and chromogranin A (Santa Cruz). The antibody raised against the 290 amino acid mouse WFS1-N-terminus has been described previously (9). Cy3- or fluorescein isothiocyanate-conjugated (FITC) secondary antibodies (Jackson Immunoresearch, West Grove, PA, USA) were used for fluorescence microscopy. Images were acquired on a confocal microscope (LSM 510, Carl Zeiss).

Evaluation of intragranular acidification

Islets were mechanically dissociated as previously described (15) to obtain dispersed islet cells. Cells were allowed to adhere on polylysine-coated plastic slides (Lab-Tek Chambered Coverglass, Nalge Nunc International, NY, USA) in RPMI medium, followed by 1 h pre-incubation with or without 100 nM bafilomycin A1 (Calbiochem) prior to DAMP and LysoTracker treatment. For DAMP staining, 3 μM DAMP (Invitrogen, OR, USA) was subsequently added to the medium for 1 h, and then dispersed islet cells were fixed with 4% paraformaldehyde in phosphate-buffered saline (PBS; pH 7.4). Anti-DNP-KLH secondary antibody (Molecular Probes, West Grove, PA, USA) was used for fluorescence microscopy. For LysoTracker (Molecular Probes) staining, 25 nM LysoTracker was added to the medium for 30 min. Then dispersed islet cells were fixed with 4% paraformaldehyde in PBS (pH 7.4). To recognize insulin-containing cells, after fixation, cells were stained with anti-insulin antibodies and visualized with FITC secondary antibodies. Fluorescent images were acquired with a confocal microscope, LSM 510 (Carl Zeiss). To measure fluorescence intensity derived from either DMAP or LysoTracker, a number of insulin-positive cells were randomly selected from both genotypes. The fluorescence intensity of each whole cell with the exception of the nucleus was measured and was later quantified using ImageJ 1.38× (36).

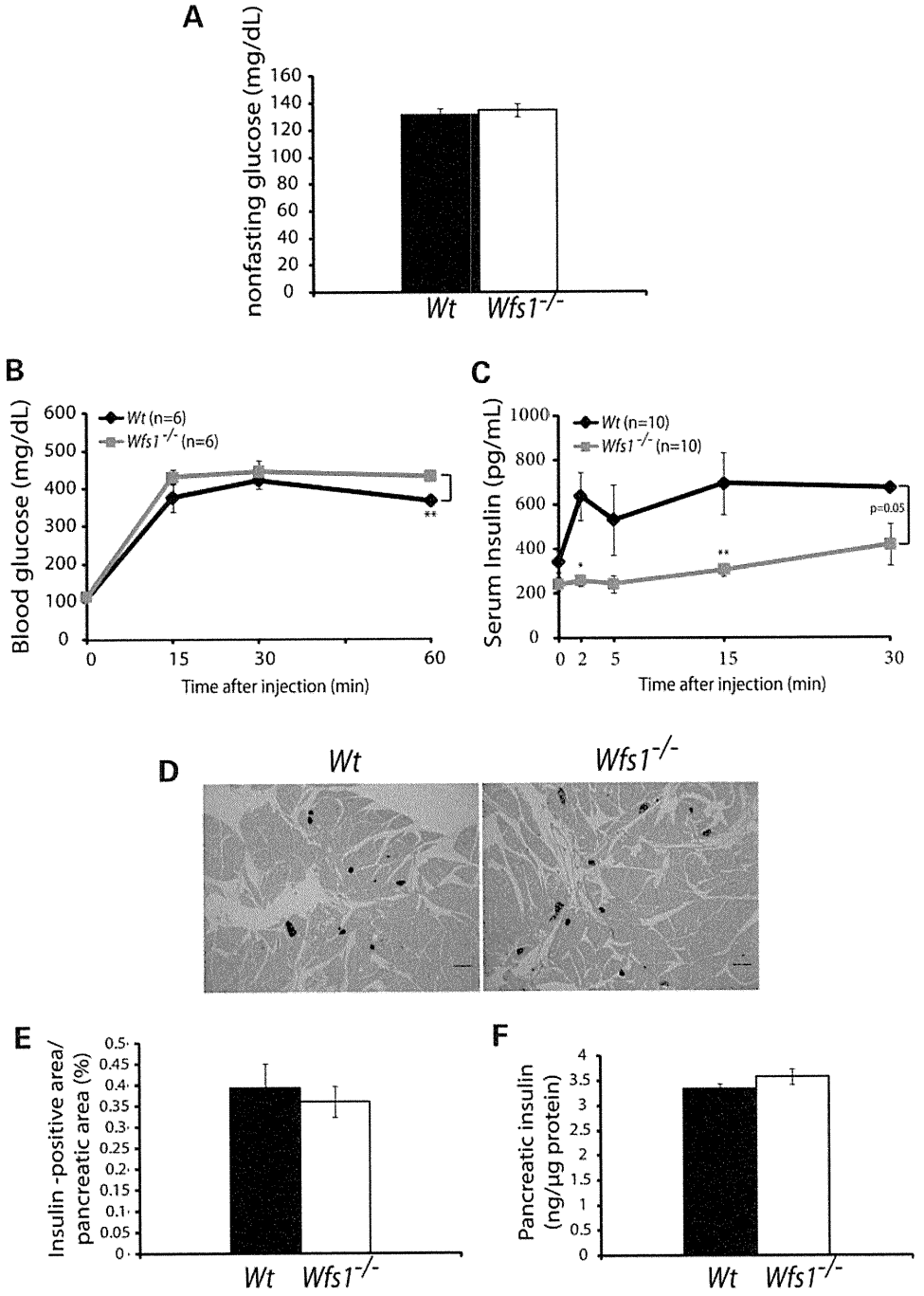

Figure 4. WFS1 deficiency results in glucose intolerance with severely impaired glucose-induced insulin release. (**A**) Non-fasting blood glucose levels in 12-week-old male mice (*Wt*, $n = 11$; *Wfs1*$^{-/-}$, $n = 11$). Intraperitoneal glucose tolerance tests were performed on overnight-fasted male *Wt* and *Wfs1*$^{-/-}$ mice at 12 weeks of age after intraperitoneal injection of D-glucose (2 g/kg) (**B** and **C**). (B) Glucose levels at the indicated time intervals. $^{*}P < 0.05$; $^{**}P < 0.01$ (*Wt*, $n = 6$; *Wfs1*$^{-/-}$, $n = 6$). (C) Plasma insulin levels at indicated time points after glucose injection (*Wt*, $n = 10$; *Wfs1*$^{-/-}$, $n = 10$). Random pancreatic sections from the entire pancreas of 12-week-old mice of the indicated genotypes were stained with antibodies to insulin and then counterstained with hematoxylin (**D** and **E**). (D) Representative photographs of indicated genotypes are shown. Scale bar represents 300 µm. (E) Insulin-immunoreactive area was measured. Results are expressed as % of total pancreatic area containing insulin-immunoreactive cells (*Wt*, $n = 3$; *Wfs1*$^{-/-}$, $n = 3$). (**F**) Insulin content extracted from whole pancreas of *Wt* and *Wfs1*$^{-/-}$ mice (*Wt*, $n = 15$; *Wfs1*$^{-/-}$, $n = 12$).

Measurement of β-cell area

All animals were anesthetized with sodium pentobarbital (65 mg/kg, intraperitoneally) and perfused intracardially with 4% paraformaldehyde. Isolated pancreatic tissues were then routinely processed for paraffin embedding, and 3 µm sections were cut and mounted on glass slides. The sections were de-paraffinized and re-hydrated, then immunostained with antibodies to insulin (Dako) bound to biotin-conjugated secondary antibodies with 3,3′-diaminobenzidine

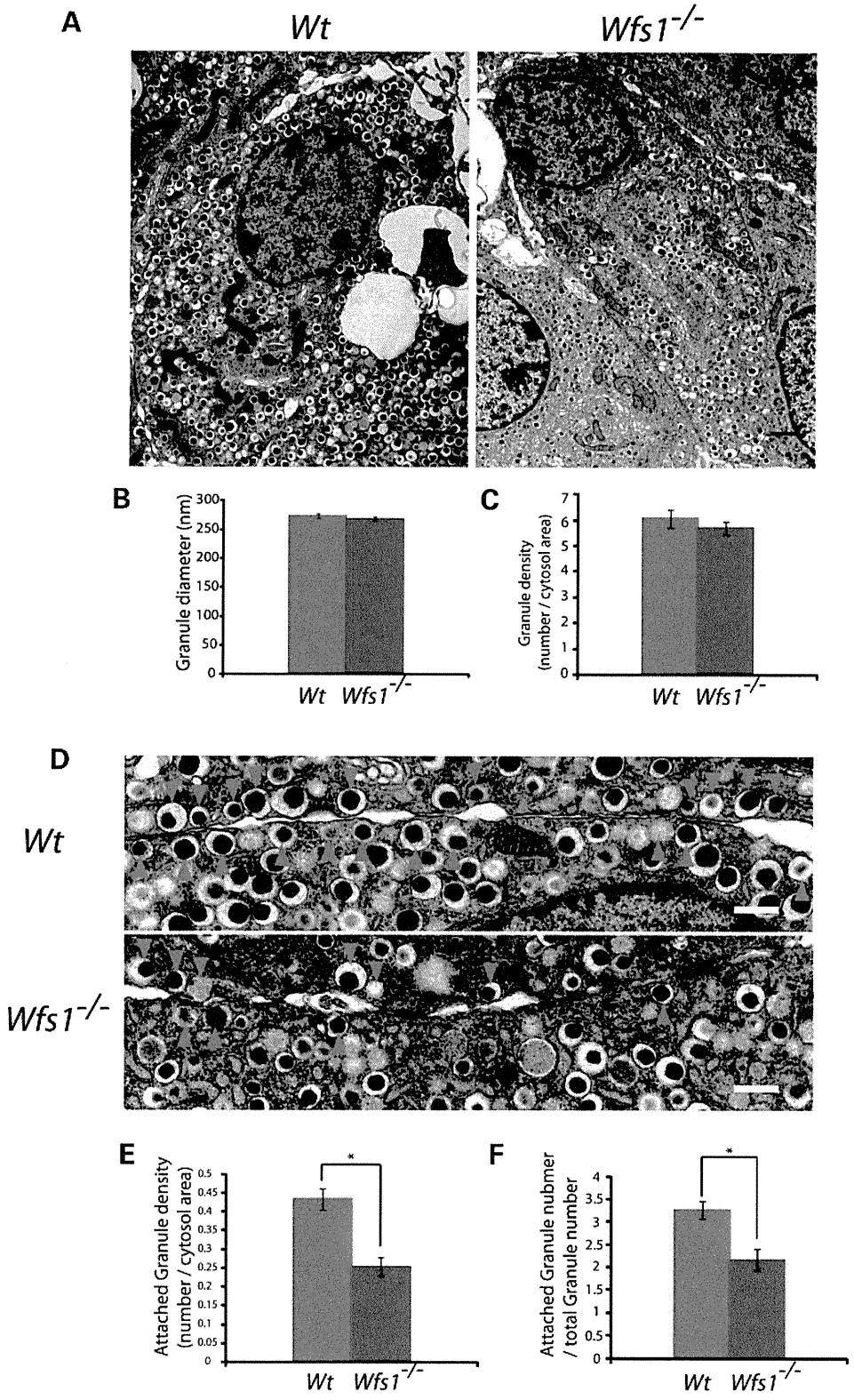

Figure 5. WFS1-deficient β-cells have reduced the number of dense-core secretory granules attached to the plasma membrane. Morphometric analyses of insulin granules in β-cells from *Wfs1*$^{-/-}$ and *Wt* mice. For each genotype, 20 randomly selected β-cells from two 12-week-old male mice were analyzed. (**A**) Electron micrographs of β-cell sections from *Wfs1*$^{-/-}$ and *Wt* mice. Scale bar represents 1 μm. (**B**) Average granule diameter and (**C**) granule number per cytosol area (μm^2). (**D**) Electron micrographs of insulin granules attached to the plasma membrane. Scale bars indicate 500 nm. (**E**) Average number of attached granules per cytosol area (μm^2) and (**F**) the attached granules to total granules ratio are summarized as the mean ± SEM in the graph. *$P < 0.05$.

tetrahydrochloride and hematoxylin. The β-cell area was determined after analysis of a number of random sections from three mice in each genotype and analyzed with ImageJ 1.38×.

Isolation of islets from mice

Islets from 12-week-old C57BL/6J male mice, *Wfs1*$^{-/-}$ and *Wfs1*$^{+/-}$/C57BL/6J background male mice were isolated by ductal collagenase digestion of the pancreas (15) followed by filtering and washing through a 70-mm Nylon cell strainer (BD Biosciences). Isolated islets were then maintained in RPMI medium containing 11 mM glucose, 10% FBS, 200 U/ml of penicillin and 200 mg/ml of streptomycin in humidified 5% CO_2 and 95% air at 37°C. All experiments on isolated islets were carried out 15 h after isolation.

Preparation of total cell extract

Isolated islets were washed twice in ice-cold PBS and lysed in ice-cold cell lysis buffer consisting of 50 mM HEPES (pH 7.5), 1% (v/v) Triton X-100, 2 mM activated sodium orthovanadate, 100 mM sodium fluoride, 10 mM sodium pyrophosphate, 4 mM EDTA, 1 mM phenylmethylsulfonyl fluoride, 1 μg/ml of leupeptin and 1 μg/ml of aprotinin, then passed through a syringe with a 21 gauge needle 10 times, and particulate material was removed by centrifugation (10 000*g* for 10 min at 4°C). The supernatant was collected. Protein concentrations were determined using the BCA protein assay (Thermo Scientific, Rockford, IL, USA).

For immunoprecipitation, mouse insulinoma MIN6 cells were cultured in 100 mm diameter culture dishes until 80% confluence and lysed in ice-cold RIPA buffer consisting of 20 mM HEPES (pH 7.2), 100 mM NaCl, 25 mM NaF, 1 mM sodium vanadate, 1 mM benzamidine, 5 μg/ml of leupeptin, 5 μg/ml of aprotinin, 1 mM phenylmethylsulfonyl fluoride, 1 mM dithiothreitol and 0.5% NP-40 in the presence of 1 mM EDTA and centrifuged for 15 min at 15 000*g*. Immunoprecipitation was performed using anti-WFS1 antibody and protein A Sepharose. After washing, immune complexes were directly eluted from the Sepharose using RIPA buffer.

Western blot analysis

Proteins were resolved on 4–20 or 15–25% gradient polyacrylamide gels (Cosmo Bio Tokyo), blotted onto a PVDF membrane (Amersham Plc, Buckinghamshire, UK) and incubated overnight at 4°C in Tris-buffered saline containing a 1:500–1000 dilution of antibodies as listed below. The membrane was then incubated at 4°C for 60 min in Tris-buffered saline with a 1:5000 dilution of anti-rabbit IgG or anti-mouse IgG horseradish peroxidase–conjugated secondary antibody (Jackson Immunoresearch). Antibodies used were anti-WFS1 (9), anti-insulin/proinsulin (Dako), anti-PC2 (Gene Tex), anti-PC1/3 (Abcam, Cambridge, UK) and anti-mGAPDH (Sigma, St Louis, MO, USA). Immune complexes were revealed using an ECL Western Blot Detection kit (Amersham Plc) and the images were acquired by exposure onto medical X-ray film (Konica Minolta). Band intensities in the blots were later quantified using ImageJ 1.38× (36), and mGAPDH bands were used to adjust for loading differences.

Electron microscopy

Conventional electron microscopy was performed as described previously (14). In brief, isolated pancreases were routinely processed. Ultrathin sections were doubly stained with uranyl acetate and lead citrate, and then observed under an electron microscope (Tecnai^{TM} G^2 Spirit, FEI Company). The diameter and the density of secretory granules were analyzed and quantified using ImageJ 1.38× (36).

Immunoelectron microscopy

All animals were anesthetized with sodium pentobarbital (65 mg/kg, intraperitoneally) and perfused intracardially with ice-cold saline, followed by 0.5% glutaraldehyde and 4% paraformaldehyde in 0.1 M phosphate buffer (PB; pH 7.4). Pancreata were removed and soaked in 0.1 M PB containing 30% sucrose until they sank, and then frozen in powdered dry ice. Pancreatic sections were cut at a thickness of 60 μm using a cryostat. The free-floating sections were pre-incubated for 2 h with 20% normal goat serum (NGS) in PBS and bleached for 1 h with 50% methanol and 1.5% hydrogen peroxide at 4°C. After washing with PBS containing 0.05% NGS and 0.3% Triton X-100, the sections were incubated with anti-WFS1 diluted 1:200 in PBS containing 1% NGS for 2 days at 20°C. Then, the sections were incubated for 2 h at 20°C with biotinylated secondary antibody (Dako Cytomation, Glostrup, Denmark; diluted 1:500) in PBS containing 1% NGS, followed by incubation with a mixture of horseradish peroxidase and rabbit anti-horseradish peroxidase antibody complexes (PAP; Dako Cytomation) and peroxidase-conjugated streptavidin (Dako Cytomation, diluted 1:500) in PBS (PAP-BAP method) for 2 h at 20°C. Subsequently, they were washed in 0.05 M Tris–HCl buffer and colored by a nickel-enhanced DAB reaction. The sections were post-fixed for 1 h with 1% OsO_4 in 0.1 M PB, block-stained for 1 h with 2% uranyl acetate in distilled water, dehydrated with a graded series of ethanol rinses, infiltrated with propylene oxide and finally embedded in epoxy resin. Ultrathin sections were collected on copper grids and observed under a Tecnai^{TM} G^2 Spirit (FEI Company) electron microscope, operated at 120 kV with 2 min of lead staining. For immune-gold-electron microscopy, the pre-embedded immunogold method was used. Cryosections (60 μm) were incubated with anti-WFS1 diluted 1:100 in PBS containing 1% NGS for 5 days at 20°C, followed by incubation with secondary antibodies conjugated with colloidal gold (10 nm diameter, BB International, diluted 1:20). Quantification of the distribution of gold particles on secretory granules and ER was performed in representative sections of a number of cells ($n = 24$).

Statistical analysis

Data were obtained from at least three independent experiments and presented as mean ± SEM. The significance of variations was analyzed by one-factor Student's *t*-test with a significance level of 0.05 (95% confidence interval).

ACKNOWLEDGEMENTS

The authors would like to thank members of the division for helpful discussion.

Conflict of Interest statement. None declared.

FUNDING

This study was supported in part by Grants-in-Aid for Scientific Research (16390096, 18390103 and 20390093 to Y.T., 22590984 to K.T., 21500326 to K.S.) from the Ministry of Education, Culture, Sports, and Science, grants (to Y.O. and Y.T.) from the Ministry of Health, Labor and Welfare of Japan, grants from the Takeda Science Foundation (to Y.T. and K.T.) and a grant from Banyu Life Science Foundation (to K.T.).

REFERENCES

1. Wild, S., Roglic, G., Green, A., Sicree, R. and King, H. (2004) Global prevalence of diabetes: estimates for the year 2000 and projections for 2030. *Diabetes Care*, **27**, 1047–1053.
2. Donath, M.Y. and Halban, P.A. (2004) Decreased beta-cell mass in diabetes: significance, mechanisms and therapeutic implications. *Diabetologia*, **47**, 581–589.
3. Rhodes, C.J. (2005) Type 2 diabetes-a matter of beta-cell life and death? *Science*, **307**, 380–384.
4. Porter, J.R. and Barrett, T.G. (2005) Monogenic syndromes of abnormal glucose homeostasis: clinical review and relevance to the understanding of the pathology of insulin resistance and beta cell failure. *J. Med. Genet.*, **42**, 893–902.
5. Barrett, T.G. and Bundey, S.E. (1997) Wolfram (DIDMOAD) syndrome. *J. Med. Genet.*, **34**, 838–841.
6. Karasik, A., O'Hara, C., Srikanta, S., Swift, M., Soeldner, J.S., Kahn, C.R. and Herskowitz, R.D. (1989) Genetically programmed selective islet beta-cell loss in diabetic subjects with Wolfram's syndrome. *Diabetes Care*, **12**, 135–138.
7. Inoue, H., Tanizawa, Y., Wasson, J., Behn, P., Kalidas, K., Bernal-Mizrachi, E., Mueckler, M., Marshall, H., Donis-Keller, H., Crock, P. *et al.* (1998) A gene encoding a transmembrane protein is mutated in patients with diabetes mellitus and optic atrophy (Wolfram syndrome). *Nat. Genet.*, **20**, 143–148.
8. Strom, T.M., Hortnagel, K., Hofmann, S., Gekeler, F., Scharfe, C., Rabl, W., Gerbitz, K.D. and Meitinger, T. (1998) Diabetes insipidus, diabetes mellitus, optic atrophy and deafness (DIDMOAD) caused by mutations in a novel gene (Wolframin) coding for a predicted transmembrane protein. *Hum. Mol. Genet.*, **7**, 2021–2028.
9. Takeda, K., Inoue, H., Tanizawa, Y., Matsuzaki, Y., Oba, J., Watanabe, Y., Shinoda, K. and Oka, Y. (2001) WFS1 (Wolfram syndrome 1) gene product: predominant subcellular localization to endoplasmic reticulum in cultured cells and neuronal expression in rat brain. *Hum. Mol. Genet.*, **10**, 477–484.
10. Takei, D., Ishihara, H., Yamaguchi, S., Yamada, T., Tamura, A., Katagiri, H., Maruyama, Y. and Oka, Y. (2006) WFS1 protein modulates the free Ca(2+) concentration in the endoplasmic reticulum. *FEBS Lett.*, **580**, 5635–5640.
11. Riggs, A.C., Bernal-Mizrachi, E., Ohsugi, M., Wasson, J., Fatrai, S., Welling, C., Murray, J., Schmidt, R.E., Herrera, P.L. and Permutt, M.A. (2005) Mice conditionally lacking the Wolfram gene in pancreatic islet beta cells exhibit diabetes as a result of enhanced endoplasmic reticulum stress and apoptosis. *Diabetologia*, **48**, 2313–2321.
12. Yamada, T., Ishihara, H., Tamura, A., Takahashi, R., Yamaguchi, S., Takei, D., Tokita, A., Satake, C., Tashiro, F., Katagiri, H. *et al.* (2006) WFS1-deficiency increases endoplasmic reticulum stress, impairs cell cycle progression and triggers the apoptotic pathway specifically in pancreatic beta-cells. *Hum. Mol. Genet.*, **15**, 1600–1609.
13. Fonseca, S.G., Fukuma, M., Lipson, K.L., Nguyen, L.X., Allen, J.R., Oka, Y. and Urano, F. (2005) WFS1 is a novel component of the unfolded protein response and maintains homeostasis of the endoplasmic reticulum in pancreatic beta-cells. *J. Biol. Chem.*, **280**, 39609–39615.
14. Akiyama, M., Hatanaka, M., Ohta, Y., Ueda, K., Yanai, A., Uehara, Y., Tanabe, K., Tsuru, M., Miyazaki, M., Saeki, S. *et al.* (2009) Increased insulin demand promotes while pioglitazone prevents pancreatic beta cell apoptosis in WFS1 knockout mice. *Diabetologia*, **52**, 653–663.
15. Ishihara, H., Takeda, S., Tamura, A., Takahashi, R., Yamaguchi, S., Takei, D., Yamada, T., Inoue, H., Soga, H., Katagiri, H. *et al.* (2004) Disruption of the WFS1 gene in mice causes progressive beta-cell loss and impaired stimulus-secretion coupling in insulin secretion. *Hum. Mol. Genet.*, **13**, 1159–1170.
16. Osman, A.A., Saito, M., Makepeace, C., Permutt, M.A., Schlesinger, P. and Mueckler, M. (2003) Wolframin expression induces novel ion channel activity in endoplasmic reticulum membranes and increases intracellular calcium. *J. Biol. Chem.*, **278**, 52755–52762.
17. Schoonderwoert, V.T. and Martens, G.J. (2001) Proton pumping in the secretory pathway. *J. Membr. Biol.*, **182**, 159–169.
18. Barg, S., Huang, P., Eliasson, L., Nelson, D.J., Obermuller, S., Rorsman, P., Thevenod, F. and Renstrom, E. (2001) Priming of insulin granules for exocytosis by granular Cl(-) uptake and acidification. *J. Cell. Sci.*, **114**, 2145–2154.
19. Ueda, K., Kawano, J., Takeda, K., Yujiri, T., Tanabe, K., Anno, T., Akiyama, M., Nozaki, J., Yoshinaga, T., Koizumi, A. *et al.* (2005) Endoplasmic reticulum stress induces WFS1 gene expression in pancreatic beta-cells via transcriptional activation. *Eur. J. Endocrinol.*, **153**, 167–176.
20. Hofmann, S., Philbrook, C., Gerbitz, K.D. and Bauer, M.F. (2003) Wolfram syndrome: structural and functional analyses of mutant and wild-type Wolframin, the WFS1 gene product. *Hum. Mol. Genet.*, **12**, 2003–2012.
21. Anderson, R.G., Falck, J.R., Goldstein, J.L. and Brown, M.S. (1984) Visualization of acidic organelles in intact cells by electron microscopy. *Proc. Natl Acad. Sci. USA*, **81**, 4838–4842.
22. Louagie, E., Taylor, N.A., Flamez, D., Roebroek, A.J., Bright, N.A., Meulemans, S., Quintens, R., Herrera, P.L., Schuit, F., Van de Ven, W.J. *et al.* (2008) Role of furin in granular acidification in the endocrine pancreas: identification of the V-ATPase subunit Ac45 as a candidate substrate. *Proc. Natl Acad. Sci. USA*, **105**, 12319–12324.
23. Davidson, H.W., Rhodes, C.J. and Hutton, J.C. (1988) Intraorganellar calcium and pH control proinsulin cleavage in the pancreatic beta cell via two distinct site-specific endopeptidases. *Nature*, **333**, 93–96.
24. Smeekens, S.P., Montag, A.G., Thomas, G., Albiges-Rizo, C., Carroll, R., Benig, M., Phillips, L.A., Martin, S., Ohagi, S., Gardner, P. *et al.* (1992) Proinsulin processing by the subtilisin-related proprotein convertases furin, PC2, and PC3. *Proc. Natl Acad. Sci. USA*, **89**, 8822–8826.
25. Zhu, X., Orci, L., Carroll, R., Norrbom, C., Ravazzola, M. and Steiner, D.F. (2002) Severe block in processing of proinsulin to insulin accompanied by elevation of des-64,65 proinsulin intermediates in islets of mice lacking prohormone convertase 1/3. *Proc. Natl Acad. Sci. USA*, **99**, 10299–10304.
26. Orci, L., Halban, P., Perrelet, A., Amherdt, M., Ravazzola, M. and Anderson, R.G. (1994) pH-independent and -dependent cleavage of proinsulin in the same secretory vesicle. *J. Cell. Biol.*, **126**, 1149–1156.
27. Guest, P.C., Abdel-Halim, S.M., Gross, D.J., Clark, A., Poitout, V., Amaria, R., Ostenson, C.G. and Hutton, J.C. (2002) Proinsulin processing in the diabetic Goto-Kakizaki rat. *J. Endocrinol.*, **175**, 637–647.
28. Renstrom, E., Eliasson, L., Bokvist, K. and Rorsman, P. (1996) Cooling inhibits exocytosis in single mouse pancreatic B-cells by suppression of granule mobilization. *J. Physiol.*, **494** (Pt 1), 41–52.
29. Renstrom, E., Eliasson, L. and Rorsman, P. (1997) Protein kinase A-dependent and -independent stimulation of exocytosis by cAMP in mouse pancreatic B-cells. *J .Physiol.*, **502** (Pt 1), 105–118.
30. Eliasson, L., Renstrom, E., Ding, W.G., Proks, P. and Rorsman, P. (1997) Rapid ATP-dependent priming of secretory granules precedes Ca(2+)-induced exocytosis in mouse pancreatic B-cells. *J. Physiol.*, **503** (Pt 2), 399–412.
31. Deriy, L.V., Gomez, E.A., Jacobson, D.A., Wang, X., Hopson, J.A., Liu, X.Y., Zhang, G., Bindokas, V.P., Philipson, L.H. and Nelson, D.J. (2009) The granular chloride channel ClC-3 is permissive for insulin secretion. *Cell Metab.*, **10**, 316–323.
32. Li, D.Q., Jing, X., Salehi, A., Collins, S.C., Hoppa, M.B., Rosengren, A.H., Zhang, E., Lundquist, I., Olofsson, C.S., Morgelin, M. *et al.* (2009) Suppression of sulfonylurea- and glucose-induced insulin secretion in

vitro and in vivo in mice lacking the chloride transport protein ClC-3. *Cell Metab.*, **10**, 309–315.
33. Zatyka, M., Ricketts, C., da Silva Xavier, G., Minton, J., Fenton, S., Hofmann-Thiel, S., Rutter, G.A. and Barrett, T.G. (2008) Sodium-potassium ATPase 1 subunit is a molecular partner of Wolframin, an endoplasmic reticulum protein involved in ER stress. *Hum. Mol. Genet.*, **17**, 190–200.
34. Yurimoto, S., Hatano, N., Tsuchiya, M., Kato, K., Fujimoto, T., Masaki, T., Kobayashi, R. and Tokumitsu, H. (2009) Identification and characterization of Wolframin, the product of the wolfram syndrome gene (WFS1), as a novel calmodulin-binding protein. *Biochemistry*, **48**, 3946–3955.
35. Fonseca, S.G., Ishigaki, S., Oslowski, C.M., Lu, S., Lipson, K.L., Ghosh, R., Hayashi, E., Ishihara, H., Oka, Y., Permutt, M.A. *et al.* (2000) Wolfram syndrome 1 gene negatively regulates ER stress signaling in rodent and human cells. *J. Clin. Invest.*, **120**, 744–755.
36. Girish, V. and Vijayalakshmi, A. (2004) Affordable image analysis using NIH Image/ImageJ. *Indian J. Cancer*, **41**, 47.

Hindawi Publishing Corporation
Experimental Diabetes Research
Volume 2011, Article ID 498460, 10 pages
doi:10.1155/2011/498460

Research Article

Frequent Loss of Genome Gap Region in 4p16.3 Subtelomere in Early-Onset Type 2 Diabetes Mellitus

Hirohito Kudo,[1] Mitsuru Emi,[2] Yasushi Ishigaki,[1] Uiko Tsunoda,[1] Yoshinori Hinokio,[1] Miho Ishii,[2] Hidenori Sato,[2] Tetsuya Yamada,[3] Hideki Katagiri,[3] and Yoshitomo Oka[1]

[1] *Division of Molecular Metabolism and Diabetes, Tohoku University Graduate School of Medicine, 2-1 Seiryo-machi, Aoba-ku, Sendai, Miyagi 980-8575, Japan*
[2] *CNV Laboratory, DNA Chip Research Institute, 1-1-43 Suehiro-cho, Tsurumi-ku Yokohama, Kanagawa 230-0045, Japan*
[3] *Department of Metabolic Diseases, Center for Metabolic Diseases, Tohoku University Graduate School of Medicine, 2-1 Seiryo-machi, Aoba-ku, Sendai, Miyagi 980-8575, Japan*

Correspondence should be addressed to Hideki Katagiri, katagiri@med.tohoku.ac.jp

Received 6 October 2010; Revised 21 February 2011; Accepted 30 March 2011

Academic Editor: Kazuya Yamagata

A small portion of Type 2 diabetes mellitus (T2DM) is familial, but the majority occurs as sporadic disease. Although causative genes are found in some rare forms, the genetic basis for sporadic T2DM is largely unknown. We searched for a copy number abnormality in 100 early-onset Japanese T2DM patients (onset age <35 years) by whole-genome screening with a copy number variation BeadChip. Within the 1.3-Mb subtelomeric region on chromosome 4p16.3, we found copy number losses in early-onset T2DM (13 of 100 T2DM versus one of 100 controls). This region surrounds a genome gap, which is rich in multiple low copy repeats. Subsequent region-targeted high-density custom-made oligonucleotide microarray experiments verified the copy number losses and delineated structural changes in the 1.3-Mb region. The results suggested that copy number losses of the genes in the deleted region around the genome gap in 4p16.3 may play significant roles in the etiology of T2DM.

1. Introduction

Type 2 diabetes mellitus (T2DM) is a common metabolic disease, affecting nearly 300 million individuals worldwide. T2DM affects over 10% of adult individuals over 40 years of age in Japan. The continuous increase in the number of patients is a major public health problem worldwide. Loci for rare monogenic forms of diabetes, such as maturity-onset diabetes of the young [1], mitochondrial diabetes [2, 3], and Wolfram syndrome [4], have been elucidated in a limited proportion of patients. However, the etiology of sporadic T2DM remains largely unknown. Accumulating epidemiological evidence [5–8] suggests that genetic factors play an important role in the susceptibility to sporadic T2DM, in addition to environmental factors such as obesity, aging, and exercise.

To search for susceptibility gene(s) for sporadic T2DM, genome-wide association studies (GWASs) using single nucleotide polymorphism (SNP) markers have been performed. These GWASs and replication studies have found multiple loci, *TCF7L2* [9], *KCNQ1* [10, 11], and others [12–18], that are associated with susceptibility to T2DM. However, the overall contribution of these SNPs to sporadic T2DM is relatively low; their odds ratio being in the range of 1.1–1.4 [9, 11]. In addition, these associations have not necessarily been replicated in subsequent studies [12–18].

Copy number variations (CNVs) or structural variations, such as deletion or gain of a genomic region, are increasingly recognized as important interindividual genetic variations across the human genome. CNVs account for more nucleotide variation between two individuals than do SNPs [19–21]. Repetitive, multicopy regions, such as segmental duplications and low copy repeats associated with CNV, are regarded as "rearrangement hotspots," and CNV regions are predisposed to the generation of deletion/duplication events [22]. Such repeat-rich regions were recently found to

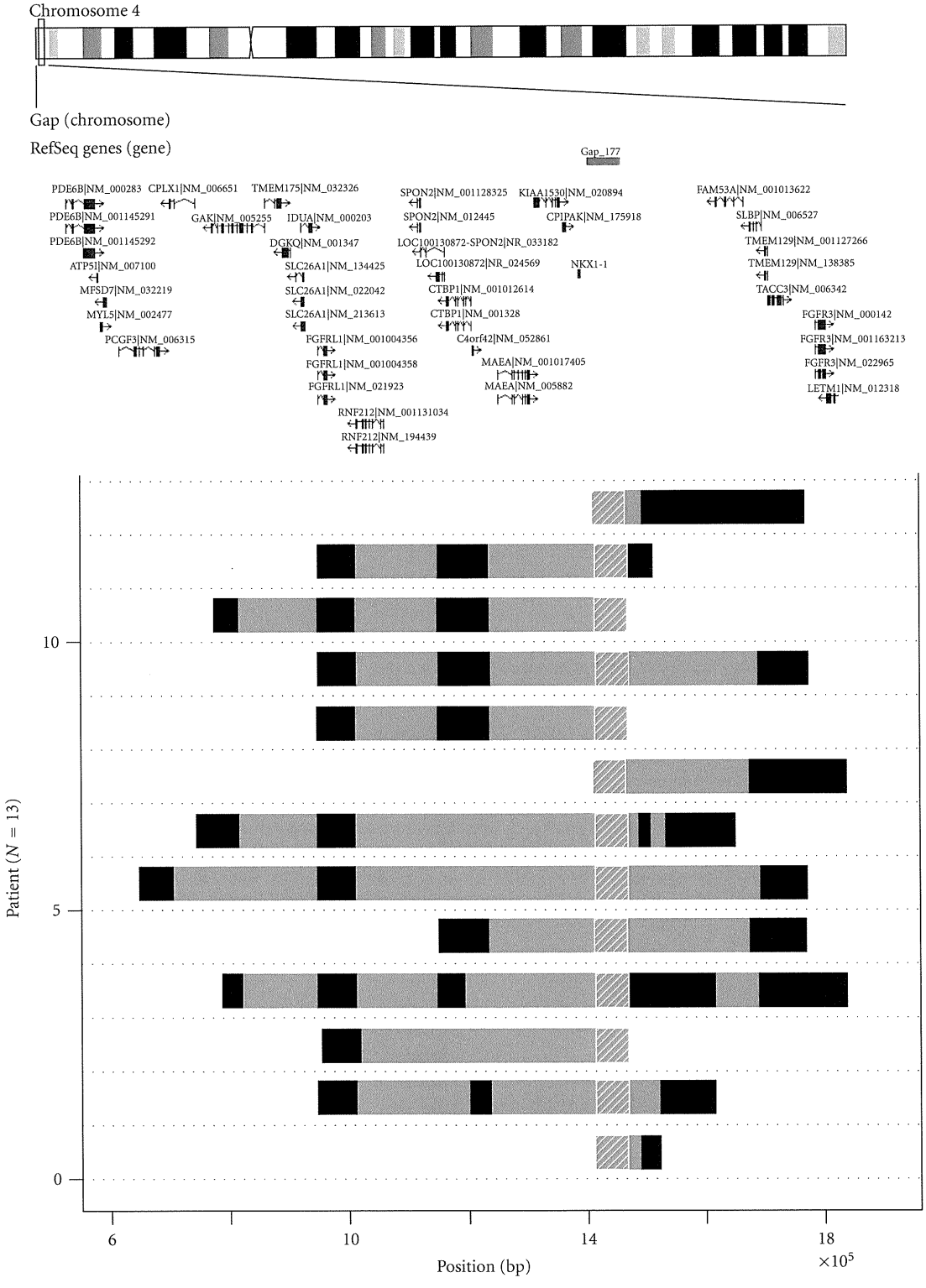

FIGURE 1: Genomic region harboring copy number loss of 1.3-Mb 4p16.3 subtelomeric region in 13 early-onset T2DM patients. Data measured by deCODE/Illumina CNV370K chip were analyzed by the PennCNV program. Genome structure of the 13 patients are aligned as horizontal bars from genome position 550,000 (left) to position 1,850,000 (right). Hatched region at position 1,423,147–1,478,646 represents genome gap-177 region. Dark solid horizontal bars represent extent of copy number loss in each T2DM patient. Gray regions between the dark bars represent intervals where copy number loss could not be inferred due to poor probe coverage. Upper map shows ideogram of chromosome 4 and the positions of putative genes in 4p16.3 region described in Database of Genomic Variants (http://projects.tcag.ca/variation/). Position is given relative to NCBI Build 35 for the chromosome 4.